Zeitschrift: IABSE congress report = Rapport du congrès AIPC = IVBH Kongressbericht

Band: 9 (1972)

Rubrik: Theme Ib: Post-critical buckling

I b
Instabilité dans le domaine post-critique
Instabilität im überkritischen Bereich
Post-Critical Buckling

Leere Seite
Blank page
Page vide

Some Practical Considerations on the Postcritical Behaviour of Structures

Quelques remarques pratiques sur le comportement des structures dans le domaine post-critique

Praktische Bemerkungen über das Verhalten der Konstruktionen im überkritischen Bereich

LAJOS KOLLÁR
Dr. techn.
Budapest, Hungary

In the following the postcritical behaviour of structures would be dealt with from the viewpoint of their practical applications.

Basically, three different types of postbuckling behaviour can be distinguished. The load-bearing capacity of the structure can be - after exceeding the critical load P_{cr}^{lin} of the classical /linear/ theory - either increasing, or constant, or decreasing. Plotting the load P against some average value of the buckling deformation w, these three cases can be represented by the diagrams of Figs. 1a,b,c. Here, in addition to the perfect /centrally compressed/ case, some curves corresponding to initially imperfect structures have been represented too.

Structures with <u>increasing</u> postbuckling load-bearing capacity /Fig. 1a/ are insensitive to initial imperfections and/or creep because their diagrams have no peak which could be influenced by these two factors. On the other hand, structures with <u>decreasing</u> diagrams /Fig. 1c/ are extremely sensitive to initial imperfections and creep as well, for the peak value of their P/w/-curves depend markedly on the magnitude of both. /The influence of creep is similar to that of initial imperfections because creep increases buckling deformation, thus it augments the influence of the imperfection./ We can thus choose a much smaller safety factor for structures corresponding to Fig. 1a than to those of Fig. 1c.

Structures corresponding to Fig. 1c form a case of transition between the two other groups. Its importance comes mainly from the fact that it can be treated theoretically in a simple way, but it also describes, at least approximatively, the behaviour of some structures /e.g. buckling of bars/.

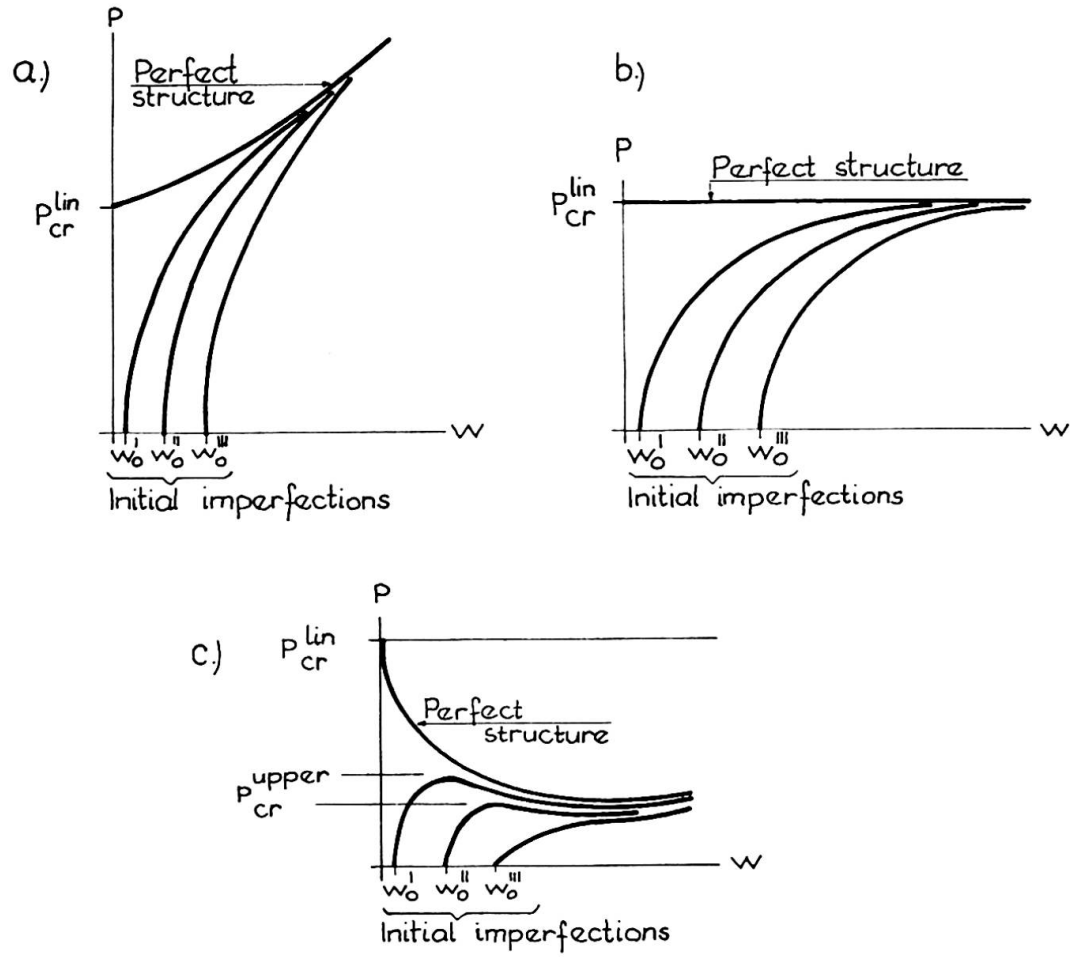

Fig. 1.

From all that has been said follows that when designing a structure, it is most important to know whether its postbuckling load-bearing capacity increases or decreases. For some structures we know this from theoretical investigations to be found in the literature. But if we have to design a structure the postbuckling analysis of which has not yet been made, some simple criteria to determine the kind of its postbuckling behaviour could be of great value. In the following some such criteria will be shown.

Theoretically it can be said [2], [3] that a structure has an increasing postbuckling load-bearing capacity if the following two conditions are fulfilled:

a/ The structure must have some parts which can bear more load, even without the other, more buckled /weaker/ parts, than the whole structure.

b/ The redistribution of stresses that is necessary for con-

dition a/ must be physically possible in the structure itself as well as at the supports.

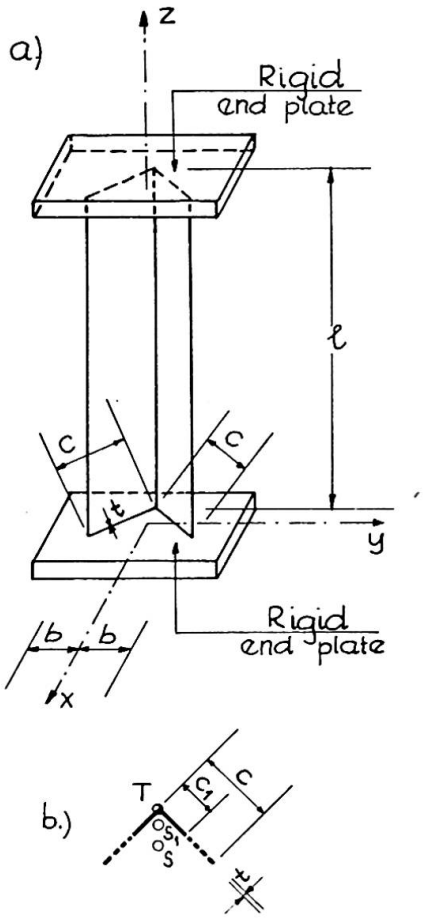

Fig 2.

Let us illustrate this on the pure torsional buckling of a straight bar with the cross section of an angle /Fig. 2a/. When the critical load is exceeded, the angle begins to buckle with the rotation of the cross sections around their shear centre T /Fig. 2b/. We can assume, as an approximation, that the free ends of the cross sections cease to bear any load. Thus, instead of the original flange width c of the angle only a part of it, of width c_1, will be effective. This part, however, can carry more load than the original whole structure. This can be seen in the formula for the critical load of torsional buckling for an angle with built-in ends 5 :

$$P_{cr} = 2 \frac{G t^3}{c} .$$

Since P_{cr} is inversely proportional to flange width c, the smaller c, the greater the critical load will be. Condition a/ is thus fulfilled.

In this case the redistribution of stresses means that the point of action of the load must shift from the original centroid S to the centroid S_1 of the smaller cross section. If the end conditions make this possible /e.g. in case of rigid end plates/, then condition b/ is also fulfilled, thus we obtain an increasing postbuckling load-bearing capacity.

Essentially the same considerations can be made in relation to the torsional buckling of shell-arches 1 , 3 , plate buckling 5 etc., i.e. in all cases where the critical load is inversely proportional to some dimension of the structure, and even in some other cases. Sometimes it is also possible to establish a simple upper bound for the maximum value of the postbuckling load the

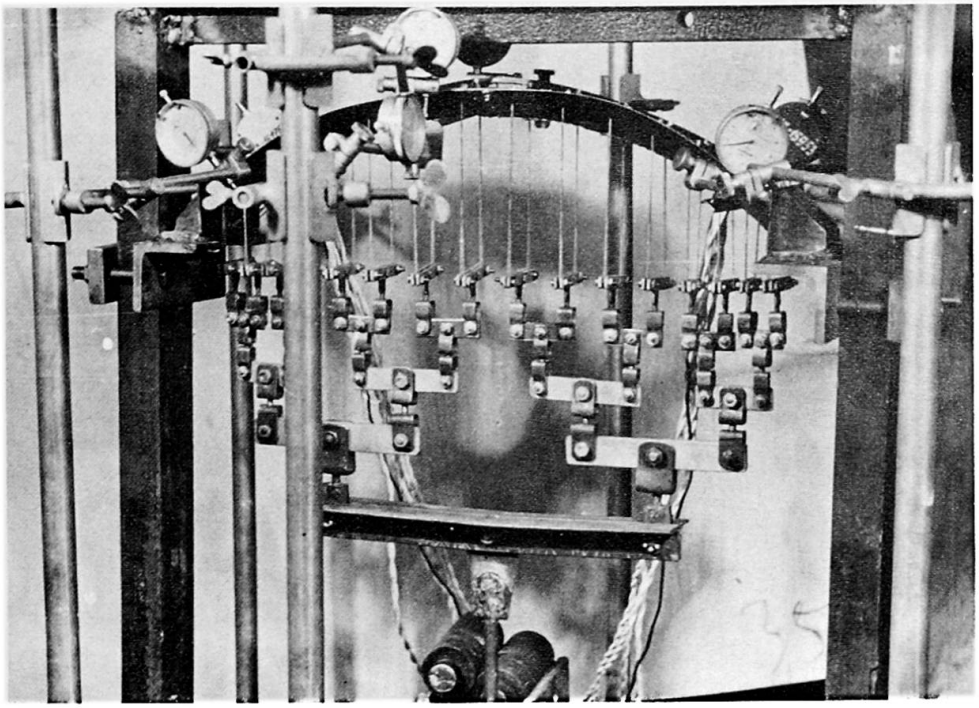

Fig. 3.

structure can carry [2]. For illustration, Fig. 3 shows a steel model of a shell-arch with built-in ends under centrical compression. The rotation of the middle cross section, as characteristic for the torsional buckling, is plotted in Fig. 4. After exceeding the linear critical load P_{cr}^{lin} = 512 kp, the load-deflection curve has a markedly ascending character, represented in Fig. 1a.

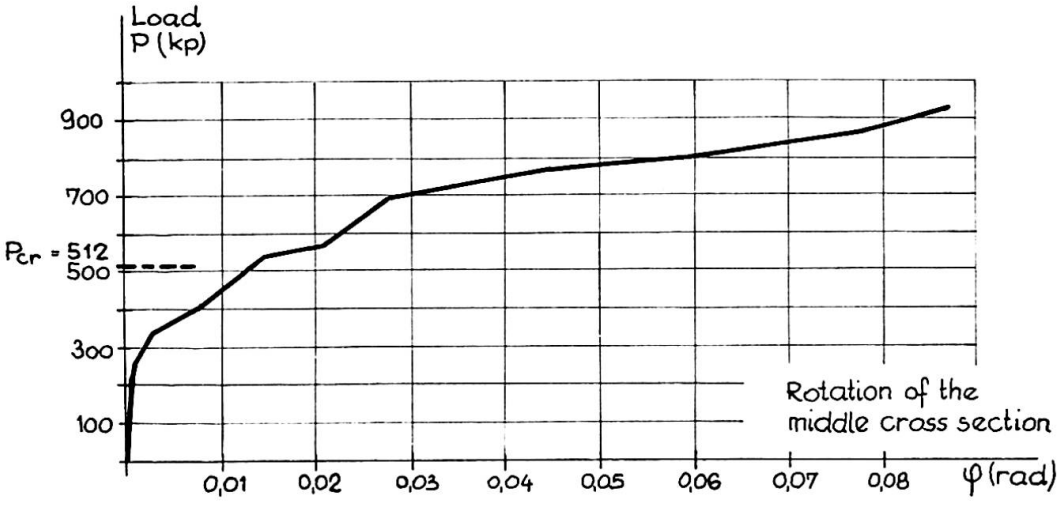

Fig. 4.

In cases, however, when these theoretical considerations cannot be applied, there is another possibility to predict postbuckling behaviour from <u>non-destructive model tests.</u>

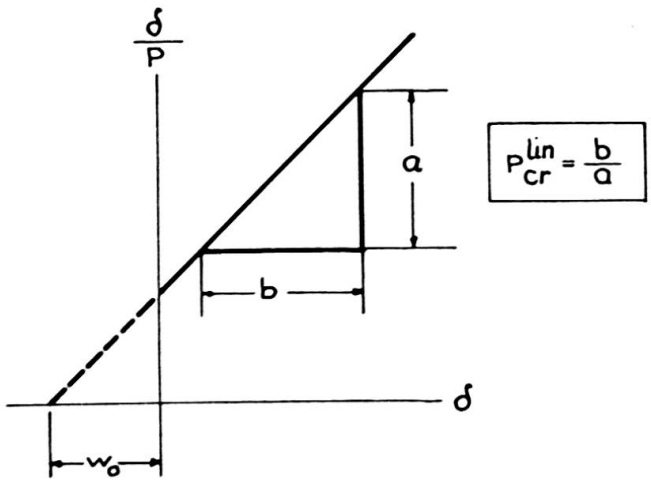

Fig. 5.

It is well known [5] that for structures corresponding to Fig. 1b, the asymptotic curves for the imperfect cases can be made straight by plotting the ratio δ/P against the buckling deformation $\delta = w - w_o$, measured from the initial /imperfect/ state w_o /Fig. 5/. The inverse slope of this line gives the critical load. This procedure, called Southwell's plot, greatly facilitates the determination of this latter since it would be much more uncertain to determine the asymptotic value of the curves in Fig. 1b by extrapolation.

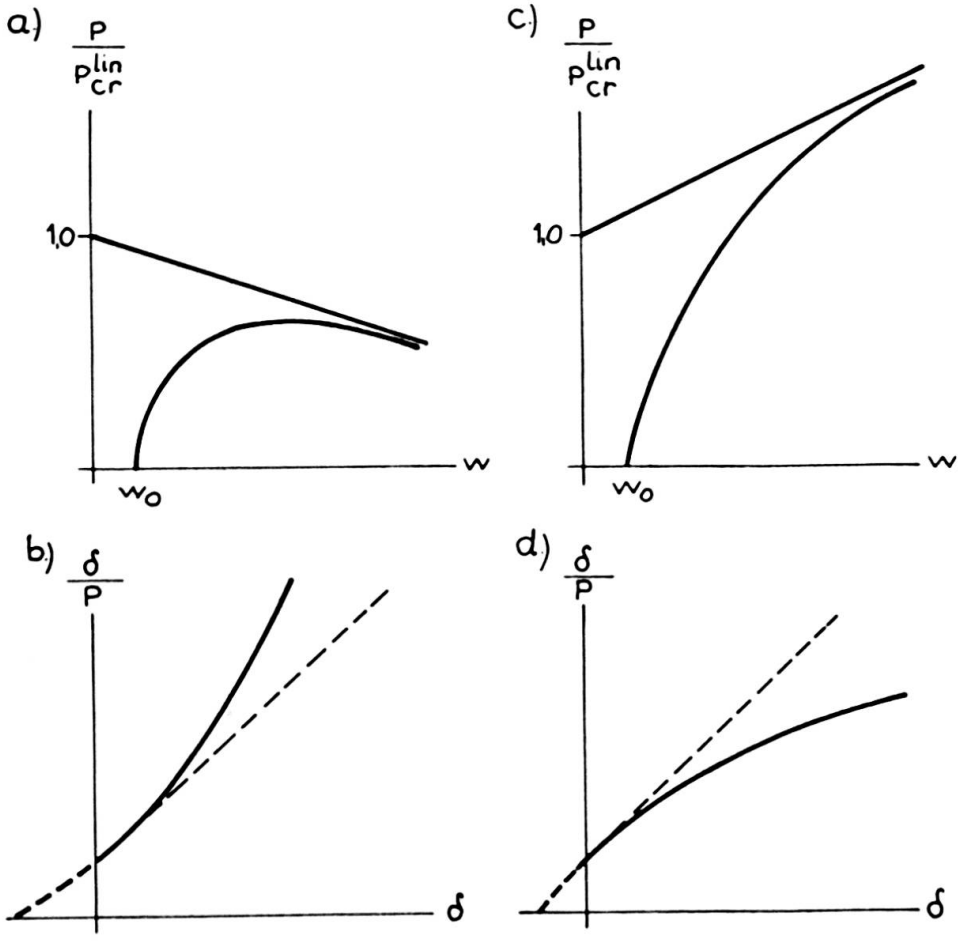

Fig. 6.

It can be easily shown [2], [4] that in case of increasing or decreasing

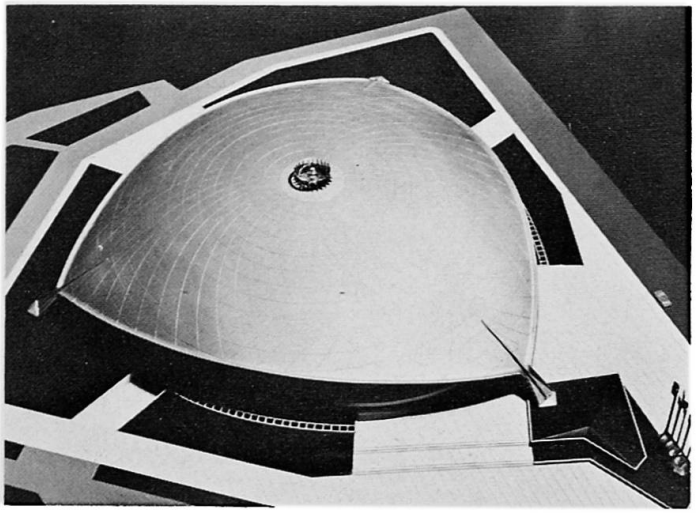

Fig. 7.

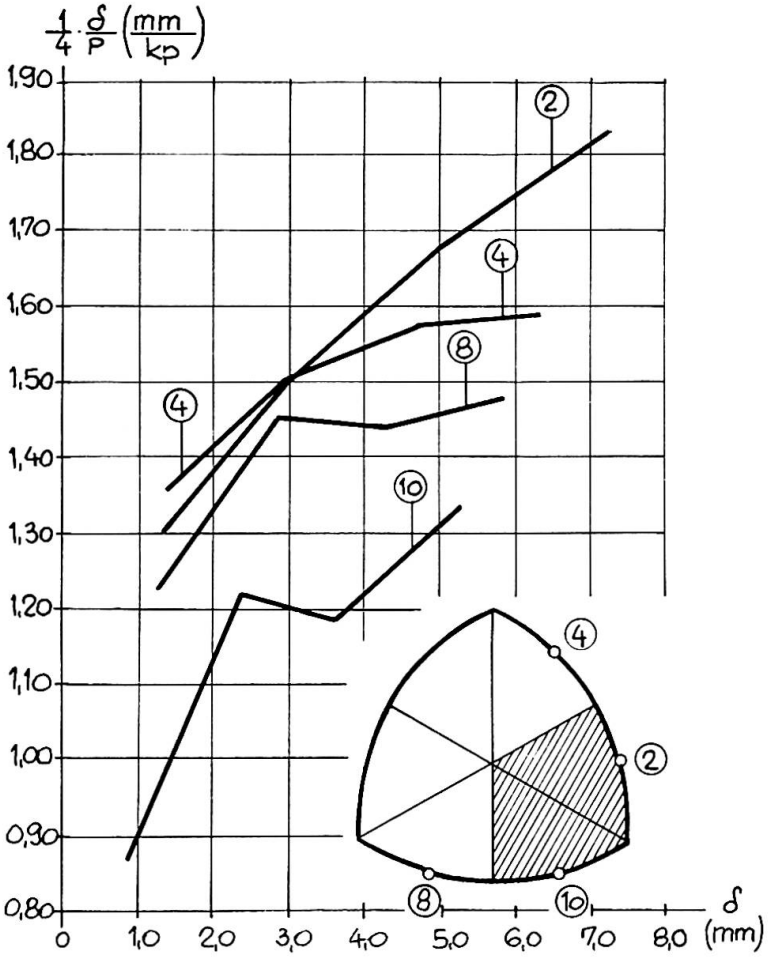

Fig. 8.

postbuckling load-bearing capacities, the Southwell diagram becomes curved downwards or upwards, respectively /Fig. 6/. Thus, measuring the buckling deformations of the model and plotting δ/P against them, we can decide at once and without destructing the model whether it has a constant /Fig. 1b/, an increasing /Fig. 1a/ or a decreasing /Fig. 1c/ postbuckling load-bearing capacity.

For illustration we show some results of the model test of the new Budapest Sports Hall, designed recently /Fig. 7/. Its structure is a reticulated steel shell without stiffening edge arches, supported by three points at a distance of 112,80 m.

For the stability of the structure only rough estimates could be

made in the course of design. Thus we had to resort to a model test. Since we intended to study its behaviour under several loading cases, it was desirable to clear up postbuckling characteristics by a non-destructive model test in order to avoid costs of several models. Fig. 8 shows the Southwell diagrams of four edge points for the loading indicated by hachure. All diagrams show a definite downward curvature. The ensuing increasing postbuckling load-bearing capacity has been confirmed by the final test when we loaded the model with total load up to failure.

I hope these viewpoints might be of some use for designers.

References

[1] Kollár, L.: On Postbuckling Behaviour of Shell-arches. Bulletin of the International Association for Shell Structures, N. 30, June 1967, 21-32.

[2] Kollár, L.: On the Behaviour of Shells in the Post-Buckling Range
Bulletin of the International Association for Shell Structures, N. 39, Sept. 1969, 41-51.

[3] Kollár, L.: Statik und Stabilität von Schalenbogen und Schalenbalken.
W. Ernst und Sohn, Berlin - Akadémiai Kiadó, Budapest, 1971.

[4] Roorda, J.: Some thougths on the Southwell plot. Journ. Eng. Mech. Div. /Proc. ASCE/ 93 EM 6, 37-48 /Dec. 1967/

[5] Timoshenko, S. - Gere, J.: Theory of Elastic Stability. McGraw-Hill, New York, 1971

Summary

After description of the three main types of postbuckling behaviour of structures two conditions, necessary for the increasing postbuckling load-bearing capacity, will be established. For determination of postbuckling behaviour from non-destructive model tests, the generalized Southwell plot will be presented.

Leere Seite
Blank page
Page vide

Überkritisches Verhalten der Stabkonstruktionen

Post-Critical Behaviour of Structures

Comportement post-critique des structures

J. SZABÓ
Prof.
Zs. GÁSPÁR
Wissenschaftlicher Mitarbeiter
Technische Universität
Budapest, Ungarn

1. Einleitung

Die auch für grosse Verschiebungen gültige Zustandsänderungs-Differentialgleichung der aus endlichen Stabelementen bestehenden Stabkonstruktionen besitzt die folgende Form /s. [1] /

$$\begin{bmatrix} \underline{\underline{D}}(\underline{u},\underline{s}) & \underline{\underline{G}}^{*}(\underline{u}) \\ \underline{\underline{G}}(\underline{u}) & \underline{\underline{F}}(\underline{u},\underline{s}) \end{bmatrix} \cdot \begin{bmatrix} d\underline{u} \\ d\underline{s} \end{bmatrix} + \begin{bmatrix} d\underline{q} \\ d\underline{t} \end{bmatrix} = \underline{\underline{0}} \qquad (1)$$

Dabei bedeuten

$$D_{jk} = \frac{\partial G_{ij}}{\partial u_k} s_i \quad ,$$

$\underline{\underline{G}}$ die geometrische Matrix der Stabkonstruktion,
$\underline{\underline{G}}^{*}$ die Transponierte von $\underline{\underline{G}}$,
$\underline{\underline{F}}$ die Nachgiebigkeits-Matrix der Stabkonstruktion,
$\underline{u}$ der Vektor der unabhängigen Verschiebungskomponenten der Knotenpunkte,
$\underline{s}$ der Vektor der inneren Kräfte und Momente,
$\underline{q}$ der Vektor der auf die Knotenpunkte wirkenden äusseren Kräfte und Momente
$\underline{t}$ der Vektor der vorgeschriebenen Relativverschiebungen der Stäbe.

Diese Gleichung auf eine einparametrige Last angewandt, lässt sich die die indifferente Last bestimmende Differentialgleichung ableiten, die im allgemeinen Falle nach einem auf die Lösung eines

Eigenwertproblems beruhenden Iterationsverfahren ausgerechnet wird. Der postkritische Zustand lässt sich nach einer modifizierten Variante des für grosse Verschiebungen ausgearbeiteten Verfahrens errechnen. Die für die einzelnen Fälle ausgearbeiteten Aufgaben wurden derart gewählt, dass die analytische Lösung bekannt sei, so konnte das allgemeine Verfahren kontrolliert werden. Es wurden ebene Aufgaben gelöst und damit nicht die numerischen Schwierigkeiten vorherrschen, wurde die Anzahl der Stabelemente nicht hoch gewählt.

2. Das Modell der Stabkonstruktion

Die Stabkonstruktion kann aus elastischen Elementen oder aus starren Elementen mit elastischen Gelenken aufgebaut werden. Die geometrische Matrix $\underline{\underline{G}}$ der Stabkonstruktion aus elastischen Elementen erhält man aus der Matrix

$$\underline{\underline{G}}_o = \left[\underline{\underline{G}}_{ij}\right] \quad , \tag{2}$$

indem die bei der Kopplung der Stabelemente zu den gleichen Verschiebungskomponenten gehörenden Spalten summiert, sodann die zu den vorgeschriebenen Verschiebungskomponenten gehörenden Spalten getrennt werden. Übrigens

$$\underline{\underline{G}}_{ij} = \begin{cases} -\underline{\underline{T}}_{jv} & \text{wenn der Anfangspunkt des j-ten Stabelements der i-te Knotenpunkt ist,} \\ \underline{\underline{T}}_{jv}\ \underline{\underline{T}}^{*}_{jk}\ \underline{\underline{B}}_{j}\ \underline{\underline{T}}_{jk} & \text{wenn der Endpunkt des j-ten Stabelements der i-te Knotenpunkt ist,} \\ \underline{\underline{0}} & \text{wenn die obigen Bedingungen nicht erfüllt sind.} \end{cases}$$

In Matrix (2) gilt

$$\underline{\underline{T}}_{jk} = \begin{bmatrix} \underline{\underline{T}}_{jok} & \underline{\underline{0}} \\ \underline{\underline{0}} & \underline{\underline{T}}_{jok} \end{bmatrix}, \qquad \underline{\underline{T}}_{jv} = \begin{bmatrix} \underline{\underline{T}}_{jov} & \underline{\underline{0}} \\ \underline{\underline{0}} & \underline{\underline{T}}_{jov} \end{bmatrix},$$

$$\underline{\underline{B}}_{j} = \begin{bmatrix} 1 & & & & \zeta_j & -\eta_j \\ & 1 & & -\zeta_j & & \xi_j \\ & & 1 & \eta_j & -\xi_j & \\ & & & 1 & & \\ & & & & 1 & \\ & & & & & 1 \end{bmatrix} \tag{3}$$

wo durch die Orthogonalmatrizen $\underline{\underline{T}}_{jok}$ bzw. $\underline{\underline{T}}_{jov}$ der im Koordinatensystem x,y,z angegebene Vektor in das zum Anfangs- bzw. zum Endpunkt gehörende lokale Koordinatensystem ξ, η, ζ gedreht wird.

Die Bedeutung der Grössen in der Übertragungsmatrix $\underline{\underline{B}}_j$ ist in Abb.1. zu sehen.

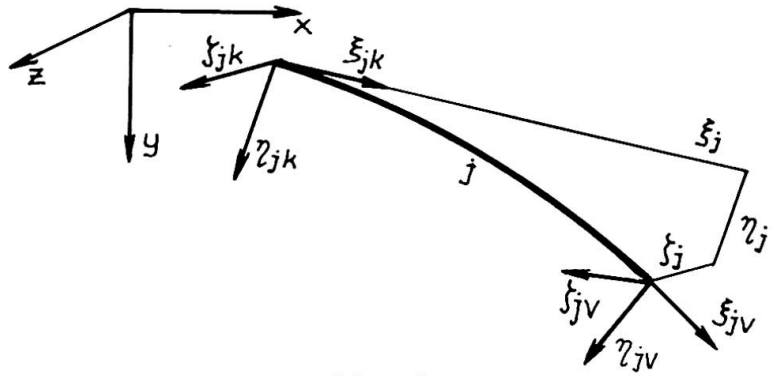

Abb. 1.

Die Nachgiebigkeitsmatrix $\underline{\underline{F}}$ ist quasi-diagonal, die einzelnen Blöcke haben die Form

$$\underline{\underline{F}}_i = \underline{\underline{T}}_{iv}\, \underline{\underline{T}}^*_{ik}\, \underline{\underline{\hat{F}}}_i\, \underline{\underline{T}}_{ik}\, \underline{\underline{T}}^*_{iv} \tag{4}$$

mit

$$\underline{\underline{\hat{F}}}_i = \begin{bmatrix} \frac{\ell}{EA} & & & & & \\ & \frac{\ell^3}{3EJ_\zeta} & & & & \frac{\ell^2}{2EJ_\zeta} \\ & & \frac{\ell^3}{3EJ_\eta} & & -\frac{\ell^2}{2EJ_\eta} & \\ & & & \frac{\ell}{GJ_\xi} & & \\ & & -\frac{\ell^2}{2EJ_\eta} & & \frac{\ell}{EJ_\eta} & \\ & \frac{\ell^2}{2EJ_\zeta} & & & & \frac{\ell}{EJ_\zeta} \end{bmatrix}_i \tag{5}$$

Wird das Modell der Stabkonstruktion durch die Kopplung von starren Elementen mit elastischen Gelenken zusammengestellt, so sind die entsprechenden Achsen der zum Anfangs- bzw. zum Endpunkt gehörenden Koordinatensysteme zueinander parallel, daher erübrigt es sich, die dazugehörige Drehmatrix zu unterscheiden /d.h. $\underline{\underline{T}}_{iv} = \underline{\underline{T}}_{ik} = \underline{\underline{T}}_i$/. Wegen der Orthogonalität der Matrix $\underline{\underline{T}}_i$

$$\underline{\underline{T}}_i\, \underline{\underline{T}}^*_i = \underline{\underline{E}} \tag{6}$$

vereinfachen sich die Beziehungen (2) und (4), und in Matrix (3) ist $\xi_j = \ell_j$, $\eta_j = \zeta_j = 0$. Sind die elastischen Gelenke gewissen Beanspruchungen gegenüber starr, so ist die Matrix $\underline{\underline{F}}$ singulär, daher müssen die in der Arbeit [2] angegebenen Transformationen durchgeführt werden.

Nach dem Iterationsverfahren in [1] können die Verschiebungen und Beanspruchungen des Modells ermittelt werden. Um das Modell und den Algorithmus zu überprüfen, wurde das Problem in Abb. 2. mit Hilfe beider Modelle gelöst. Die Angaben wurden so angesetzt, dass in der genauen Lösung, der Kragträger Viertelkreisform habe. Der spezifische Wert des Endpunkt verschiebungsfehlers ist in Abb.3. über der Elementenanzahl dargestellt /in der Abbildung bedeuten ε den Endpunktverschiebungsfehler und r den Kreisbogenhalbmesser./

Abb. 2.

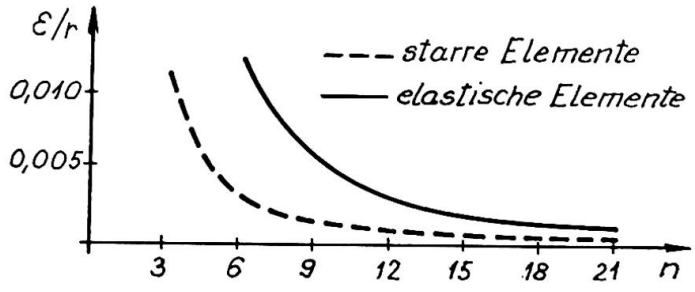

Abb. 3.

3. Stabilitätsnachweis

Der kritische Parameter einer einparametrigen Last der Stabkonstruktion wurde nach der Arbeit [3] ermittelt. Wird als Last keine relative Verschiebung vorgeschrieben, so lautet bei einer Einparameterlast die Zustandsänderungs-Differentialgleichung (1)

$$\begin{bmatrix} \underline{\underline{D}}(\underline{u},\underline{s}) & \underline{\underline{G}}^{*}(\underline{u}) \\ \underline{\underline{G}}(\underline{u}) & \underline{\underline{F}}(\underline{u},\underline{s}) \end{bmatrix} \begin{bmatrix} d\underline{u} \\ d\underline{s} \end{bmatrix} + dR \begin{bmatrix} \underline{f} \\ \underline{0} \end{bmatrix} = \underline{0} \tag{7}$$

wo

$$D_{jk} = \frac{\partial G_{ij}}{\partial u_k} s_i + R \frac{\partial f_j}{\partial u_k}$$

und

$$\underline{f} = \underline{f}(\underline{u})$$

$$\| \underline{f} \| = \text{const}$$

eine eindeutige Funktion ist.

Beim Angriff der kritischen Last hat der homogene Teil der Differentialgleichung (7) auch eine von der trivialen verschiedene Lösung, die zum Eigenwertproblem

$$\left(\left[\frac{\partial \underline{\underline{G}}^{*}}{\partial \underline{u}} \underline{s} \right] + R \frac{\partial \underline{f}}{\partial \underline{u}} - \underline{\underline{G}}^{*} \underline{\underline{F}}^{-1} \underline{\underline{G}} \right) d\underline{u} = \underline{0} \tag{8}$$

führt.

Da sowohl die Matrix $\underline{\underline{G}}$ als auch die Vektoren $\underline{\underline{f}}$ und $\underline{\underline{s}}$ Funktionen von R sind, lässt sich das Eigenwertproblem nicht direkt bestimmen. Ist der zum Parameter R_i gehörende Zustandsvektor bekannt, werden die veränderlichen Grössen des Eigenwertproblems (8) nach dem Verschiebungsvektor in eine Taylorsche Reihe entwickelt und nur deren erste zwei Glieder berücksichtigt, so erhält man das verallgemeinerte Eigenwertproblem

$$\left(\underline{\underline{A}} + R\underline{\underline{B}}\right) d\underline{\underline{u}} = \underline{\underline{0}} \tag{9}$$

das bereits direkt gelöst werden kann, wo

$$\underline{\underline{A}} = \underline{\underline{D}}_1 + \underline{\underline{D}}_3 - R_i\left(\underline{\underline{D}}_2 + \underline{\underline{D}}_2^* + \underline{\underline{D}}_4\right)$$

$$\underline{\underline{B}} = \underline{\underline{D}}_2 + \underline{\underline{D}}_2^* + \underline{\underline{D}}_4 + \underline{\underline{D}}_5$$

$$\underline{\underline{D}}_1 = -\underline{\underline{G}}_i^* \, \underline{\underline{F}}^{-1} \, \underline{\underline{G}}_i$$

$$\underline{\underline{D}}_2 = -\left(\frac{\partial \underline{\underline{G}}^*}{\partial \underline{\underline{u}}}\bigg|_{\underline{\underline{u}}=\underline{\underline{u}}_i}\left(\underline{\underline{H}}^{-1}\underline{\underline{f}}_i\right)\right)\underline{\underline{F}}^{-1}\,\underline{\underline{G}}_i$$

$$\underline{\underline{D}}_3 = \left[\frac{\partial \underline{\underline{G}}^*}{\partial \underline{\underline{u}}}\bigg|_{\underline{\underline{u}}=\underline{\underline{u}}_i}\underline{\underline{s}}_i\right]$$

$$\underline{\underline{D}}_4 = -\left[\frac{\partial \underline{\underline{G}}^*}{\partial \underline{\underline{u}}}\bigg|_{\underline{\underline{u}}=\underline{\underline{u}}_i}\left(\underline{\underline{F}}^{-1}\underline{\underline{G}}_i\underline{\underline{H}}^{-1}\underline{\underline{f}}_i\right)\right]$$

$$\underline{\underline{D}}_5 = \frac{\partial \underline{\underline{f}}}{\partial \underline{\underline{u}}}\bigg|_{\underline{\underline{u}}=\underline{\underline{u}}_i}$$

$$\underline{\underline{H}} = -\underline{\underline{D}}_1 - \underline{\underline{D}}_3 - R_i\underline{\underline{D}}_5$$

Ist der Wert $|R - R_i|$ höher als ein vorgeschriebener Wert, so wird der Zustandsvektor für einen Parameterwert R_i bestimmt, der dem kritischen Parameterwert näher liegt und das Verfahren wird wiederholt.

Wenn beim Angriff der kritischen Last nur eine geringe oder gar keine Formänderung entsteht, so ist das Eigenwertproblem (9) nur einmal zu lösen und auch die Koeffizientenmatrizen werden aus weniger Gliedern bestehen.

Zur Überprüfung des Algorithmus wurde der Stabilitätsnachweis des Bogenträgers der Form einer Parabel zweiten Grades in Abb. 4 mit Hilfe eines Modells aus starren Elementen durchgeführt. Der Parameter der kritischen Last änderte sich in Abhängigkeit von der Teilungszahl nach Abb.5.

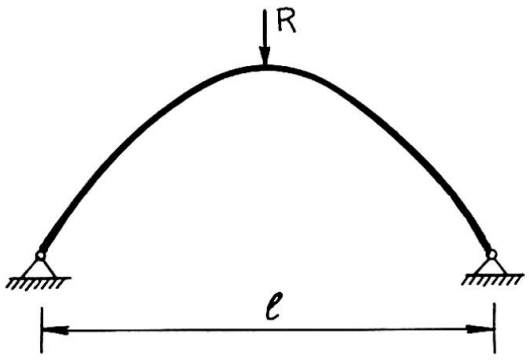

Abb.4.

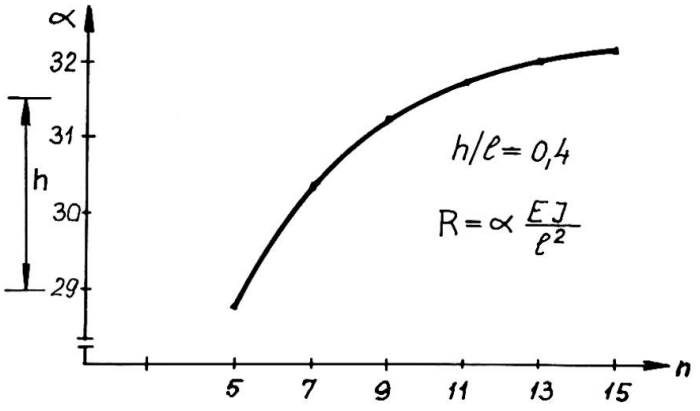

Abb.5.

4. Postkritischer Zustand bei Stabilitätsverlust ohne Verzweigungspunkt

Die Zustandsänderungskurve des Problems in Abb.6. lässt sich auch in Umgebung des Durchschlagpunktes ohne Schwierigkeit auch auf analytischem Wege ermitteln /z.B. [4] und [5] /, wenn die Biegesteifigkeit der Stäbe im Vergleich zur Normalsteifigkeit genügend gross ist und der Durchschlag ohne Stabknickung erfolgt. Das Trägermodell wird aus 6 elastischen Stabelementen gleicher Länge aufgebaut. Jeder beliebige Punkt im Abschnitt AB der Zustandsänderungskurve in Abb.7. lässt sich mit Hilfe der obenerwähnten iterativen Lösung der Differentialgleichung (7) für grosse Verschiebungen ermitteln.

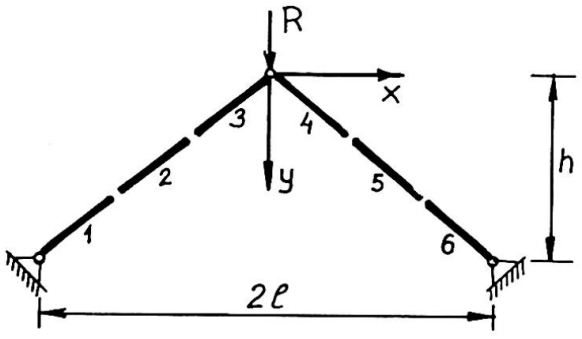

Abb.6.

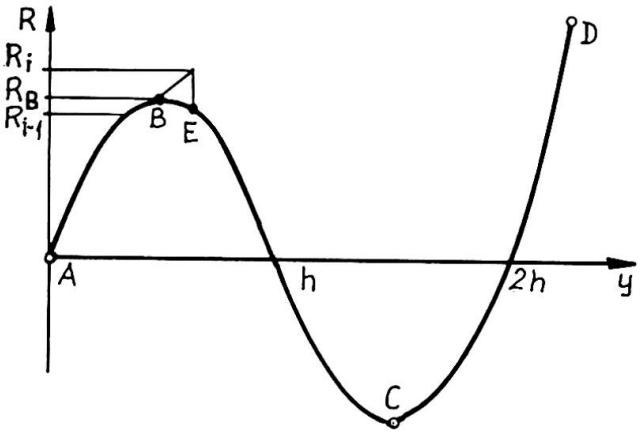

Abb.7.

Da der Wert R_B unbekannt ist und die Last stufenweise auf den Träger aufgebracht wird, kann es vorkommen, dass ein, zum Parameterwert $R_i > R_B$ gehörender Zustandsvektor gesucht wird, der lediglich mit einer ganz anderen Geometrie des Trägers ausgeglichen werden kann, daher wird beim Iterationsverfahren die Fehlervektornorm die Laststufennorm wesentlich übersteigen und die Iteration nicht konvergieren. Dafür wird durch das folgende Verfahren Ab-

hilfe geschafft, das sich um die Konvergenz zu beschleunigen auch dann verwenden lässt, wenn einige - jedoch nicht genau bestimmte - Punkte der zum Parameter R gehörenden Zustandsänderungskurve ermittelt werden sollen.

Wird die Differentialgleichung (7) als Differenzgleichung auf die Laststufe angewandt, so kann in Kenntnis der erhaltenen geometrischen Lage und der inneren Kräfte, der Vektor der äusseren Kräfte, die ausgeglichen werden können, in der Form

$$\underline{\underline{q}}^{(1)} = - \underline{\underline{G}}^{*} \underline{\underline{s}}$$

errechnet werden. Der Parameter R wird derart gewählt, dass $\| \underline{\underline{q}}^{(1)*} - R\underline{\underline{f}} \|$ minimal sei. Dies wird durch den Parameter

$$R = \frac{\underline{\underline{q}}^{(1)*} \underline{\underline{f}}}{\underline{\underline{f}}^{*} \underline{\underline{f}}} \qquad (10)$$

erfüllt. Wird der Parameter R jeweils so bestimmt, so erhält man den Punkt E in Abb.7. Soll der Parameter wieder vergrössert werden, so geht man auf der Zustandsänderungskurve nach Punkt B aus, der Parameter muss also auf dem labilen Abschnitt vermindert werden. Ob der so bestimmte Punkt auf dem labilen oder auf dem stabilen Zweig liegt, wird nach dem Energieprinzip festgestellt. Die Verschiebung unter Einwirkung des Lastzuwachses $\Delta R\underline{\underline{f}}$ /$\Delta R > 0$/ ergibt sich mit der Genauigkeit der Theorie zweiter Ordnung zu

$$\Delta \underline{\underline{u}} = \Delta R \, \underline{\underline{H}}^{-1} \underline{\underline{f}}$$

die Arbeit der Last $R\underline{\underline{f}}$ beträgt bei dieser Verschiebung

$$L = R\underline{\underline{f}}^{*} \Delta \underline{\underline{u}} \, .$$

Ist $L > 0$, so ist das Vorzeichen für ΔR gleich dem Vorzeichen von R zu wählen; ist $L < 0$, so wird für ΔR das entgegengesetzte Vorzeichen wie das von R genommen. Kurz, gilt $\underline{\underline{f}}^{*} \underline{\underline{H}}^{-1} \underline{\underline{f}} > 0$, so liegt der Punkt im stabilen, gilt $\underline{\underline{f}}^{*} \underline{\underline{H}}^{-1} \underline{\underline{f}} < 0$, so liegt der Punkt im labilen Kurvenzweig. Im indifferenten Zustand ist die Matrix $\underline{\underline{H}}$ singulär.

Der Konvergenzradius des Iterationsverfahrens ist dem Krümmungsradius der Zustandsänderungskurve proportional, so kann die Berechnung in jedem Schritt mit einer grossen Laststufe begonnen werden, nimmt jedoch die Fehlervektornorm innerhalb einiger Schritte nicht wesentlich ab, so muss die Schrittgrösse vermindert

werden. In Abb.7. wurde für $h=0,375\,\ell$ der Kurvenabschnitt AD - bei in 40 Stufen aufgetragener Last - bestimmt.

5. Postkritischer Zustand nach dem Verzweigungspunkt

Wird das Modell des Trägers in Abb.6. nur aus durch biegungselastische Gelenke verbundenen Stabelementen aufgebaut, so kann der Durchschlag lediglich mit Knickung erfolgen.

Bei einer Last unter der kritischen, tritt keine Formänderung ein, so hat das Eigenwertproblem (9) die Form

$$(\underline{\underline{D}}_1 + R\underline{\underline{D}}_5)d\underline{u} = \underline{0}$$

Der kleinste Eigenwert gibt die erste kritische Last, durch den dazugehörenden Eigenvektor wird die Knickform von einem freien Parameter abgesehen bestimmt. Um die Punkte der zur Knickform gehörenden Zustandsänderungskurve nach dem Verzweigungspunkt zu bestimmen, muss auf dem Träger das Skalarfache der durch den Eigenvektor bestimmten Form erzeugt werden. Die richtige Annahme des Skalarparameters ist von grosser Wichtigkeit,da bei einem zu niedrigen Parameterwert, die Matrix $\underline{\underline{H}}$ schlecht konditioniert /ill-conditioned/ ist, und das für die Elimination des Fehlervektors, zufolge der eingeschalteten endlichen Verschiebung, erforderliche Iterationsverfahren nicht konvergiert. Wird der Skalar zu hoch gewählt, so ist die Fehlervektornorm grösser als der Konvergenzradius.

Mit richtigen Werten gerechnet und durch die in Punkt 4 beschriebene Minimalisierung des Fehlervektors erhält man einen Punkt der Zustandsänderungskurve. Das Vorzeichen von ΔR, wieder dementsprechend angenommen, ob der Punkt auf dem stabilen oder auf dem labilen Abschnitt liegt, können die Punkte der Zustandsänderungskurve nach dem für die grossen Verschiebungen gültigen Verfahren, mit beliebiger Dichte ermittelt werden.

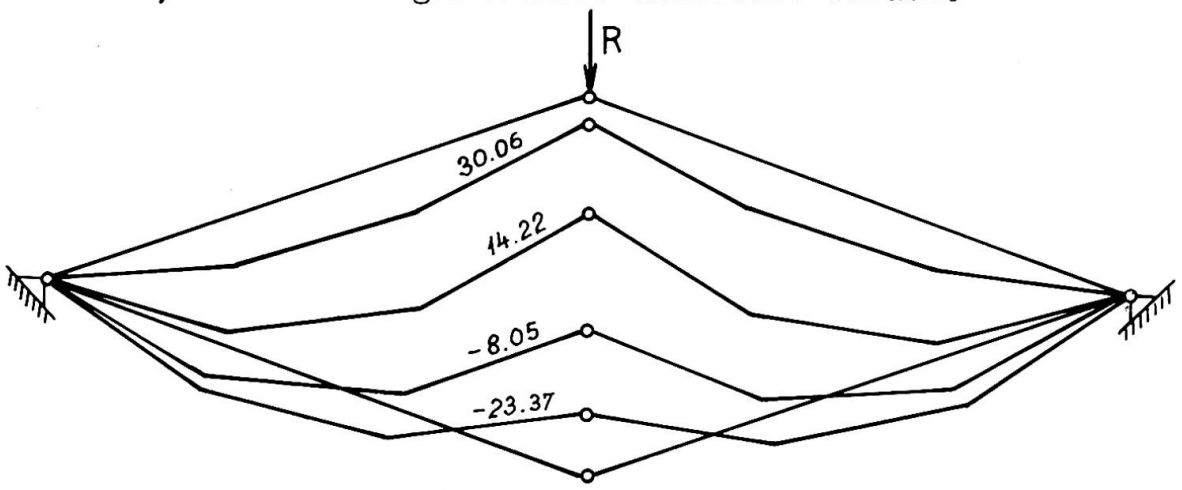

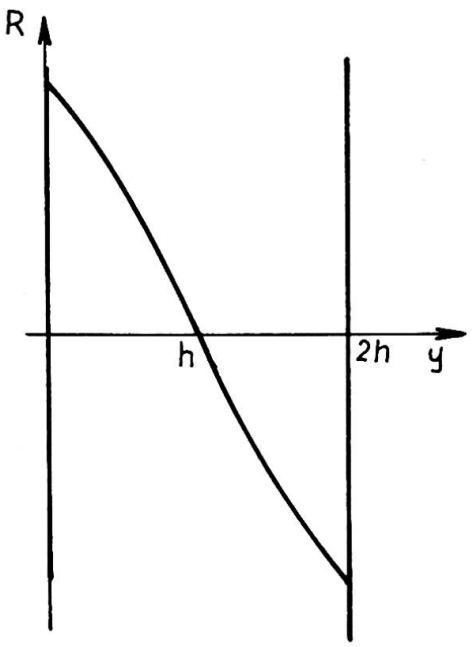

Abb.9.

Abb.8. zeigt den Träger im ursprünglichen und im Endzustand, der nach einer, mit einem Eigenvektor der Norm 0,2 begonnenen Iteration berechnet wurde, weiterhin einige Zwischenzustände des Durchschlags, wobei die jeweiligen Grössen der Ausgleichkraft angegeben sind.In Abb.9. ist die Grösse der Ausgleichkraft in Abhängigkeit von der Verschiebung des Gelenks C dargestellt.

Literatur

[1] Szabó,J.-Rózsa,P.: Grosse Verschiebungen von Stabkonstruktionen. /Acta Technica Acad.Sc.Hungaricae, im Druck/.

[2] Szabó,J.-Rózsa,P.: Die Matrizengleichung von Stabkonstruktionen. /Acta Technica Acad.Sc.Hungaricae, Tomus 71, Fasc.1-2. 1971. Budapest/.

[3] Gáspár,Zs.: Stabilitätsprüfung von Stabkonstruktionen. /Acta Technica Acad.Sc.Hungaricae, im Druck/.

[4] Falk, S.: Technische Mechanik, Dritter Band. /Springer-Verlag 1969. Berlin-Heidelberg-New York/.

[5] Kollbrunner,C.F.-Meister,M.: Knicken, Biegedrillknicken, Kippen. /Springer-Verlag p.322 1961.Berlin-Göttingen-Heidelberg/.

Zusammenfassung

Durch die Lösung eines Eigenwertproblems, das aus der Zustandsänderungs-Differentialgleichung einer mit starren oder elastischen Stabelementen modellierten, durch einparametrige Belastung belasteten Stabkonstruktion folgt, lassen sich der Parameter der kritischen Last und das Affinbild der Knickform bestimmen. Die Punkte der Zustandsänderungskurve werden numerisch mit Hilfe eines konvergenten Iterationsverfahrens bestimmt.

Leere Seite
Blank page
Page vide

Post-Critical Behaviour of Inelastic Structures

Comportement post-critique de structures non-élastiques

Überkritisches Verhalten unelastischer Träger

GIULIANO AUGUSTI
Assoc. Professor of Structural Engineering
Università di Firenze
Florence, Italy

As illustrated by Professor Bieniek's Report, it is now increasingly recognized that in structural engineering the knowledge of the post-critical behaviour is almost as essential as that of the critical load itself: in fact, the unavoidable imperfections that make actual structures different from the "ideally perfect" models of applied mechanics, affect their strength in a way that depends largely on the post-critical behaviour of their "ideally perfect" models.

This contribution presents an elementary (but hopefully stimulating) discussion of the joint effects of imperfections and inelastic deformations on the behaviour of structures that, if perfect, would exhibit a point of bifurcation of equilibrium. As in Ref. (A.1) (°), buckling will be used as a synonym for bifurcation of equilibrium, while collapse load will indicate a (local) maximum on an actual load-deformation path. Dynamical and time-rate effects will not be considered.

The most rational approach to the study of the effect of imperfections on structural strength is through statistics and probability theory, as indicated by Bieniek (p.38) and proved by an increasing number of research papers. From this point of view, an actual structure is seen as a sample structure taken out of a population of nominally identical structures, different from each other because of random variations of the design parameters (yield stress, geometric dimensions, etc.). The ideal structure, corresponding exactly to the design, is the average structure of this population. With some qualifications (°°), it can be stated that the average (expected) strength of the actual structure is approximately equal to the strength of the average structure in absence of phenomena of geometrical instability, and is lower if these phenomena are present. In the latter case, the introduction of probabilistic methods becomes of utmost importance in order to obtain economical and reliable designs. This point is illustrated, in the following Section 1, by the summary of a probabilistic investigation

---

(°) See list of References at the end of this contribution.

(°°) The following statement is too general to be more than an approximation. For instance, it has already been proved (A.2) that the average plastic collapse load of a ductile structure is smaller than the collapse load of the average structure, but in the first numerical examples their difference is rather small.

of slender imperfect columns, fully published elsewhere (A.3). A basic difference between this study and previous works by other Authors is the introduction of other random quantities (namely, the yield stress and the free buckling length) besides the geometrical imperfections.

In Ref. (A.3), collapse occurs because inelastic deformations develop: this appears to be the most frequent cause of collapse of actual structures, and it is rather surprising that the interaction of inelasticity and instability is still a comparatively little-explored field, perhaps avoided by most researchers because of its great analytical difficulties.

Section 2 below presents two examples of asymmetric behaviour (i.e., of load-deformation paths that depend on the sign of the deformation) of structures that, if perfect, would buckle elastically. In the first example, the asymmetry occurs in the inelastic range of deformations and is due to an asymmetry in the strength of structural cross-section. The second example illustrates asymmetric elastic buckling, a phenomenon now well known, after the great amount of research spurred by Koiter's fundamental works (Bieniek's Refs. 47 and 71), and apparently the only practically significant case in which collapse may be completely independent of the onset of inelastic deformations.

Finally, the last Section of this paper discusses and compares different cases of buckling in the inelastic range. Again, it will be shown that either a strength asymmetry or a geometry effect may cause asymmetry of the post-buckling load-deformation paths of the "perfect" structure: consequently, in such cases the collapse load of the actual structure depends on the sign of the imperfection.

1) ELASTIC BUCKLING AND PLASTIC COLLAPSE: A PROBABILISTIC ANALYSIS

Consider a simple compressed strut, for instance pin-ended as in Fig. 1.1, and made of an elastic-perfectly plastic material with yield stress σ_y. If the strut is initially perfectly straight, it is well known that it remains

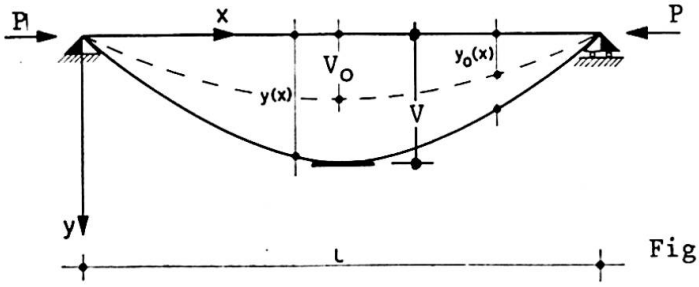

Fig. 1.1

straight and stable as long as the compressive load P is smaller than both the elastic buckling load

$$P_E = \pi^2 EI/l^2 = \pi^2 EA/\lambda^2 = \sigma_E A \quad \text{and the squash load} \quad P_y = \sigma_y A$$

If $P_E < P_y$, the load remains constant at $P = P_E$ (within the first-order, small-displacements theory) in the early stages of buckling, and begins decreasing as soon as the first plastic deformations take place; the axial load vs. mid-span displacement (P-V) path remains below, and tends asymptotically to, the P-V curve corresponding to full yielding of the cross-section $V = M_p/P$ (Fig. 1.2a): both curves have a horizontal asymptote at P = 0.

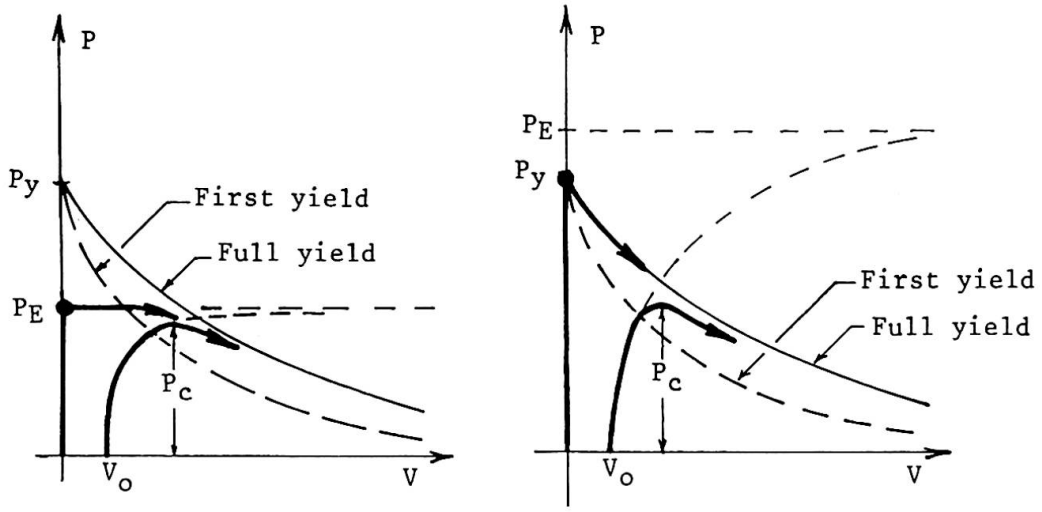

Fig. 1.2

If $P_y \leq P_E$, the strut buckles at $P = P_y$; the load P starts decreasing quite rapidly at the very onset of the deformations following the full-yield curve, and again tends asymptotically to zero when $V \to \infty$ (Fig. 1.2b).

If the material has a constant, non-zero tangent modulus E_T in the inelastic range, the horizontal asymptotes are at the load $P = P_K$ (defined in Section 3) rather than at $P = 0$ (A.4).

If the strut is affected by an initial geometrical imperfection, for instance in the form of a half sine-wave

$$Y_o = Y_o(x) = V_o \sin \pi x/l \tag{1.1}$$

(Fig. 1.1), the P-V path in the elastic range is given, with very good approximation, by (Fig. 1.2)

$$V = V_o / (1-P/P_E) \tag{1.2}$$

The actual elastic-plastic path remains below the full-yield curve: collapse occurs when sufficient plastic deformations have developed. The relation between imperfection magnitude and collapse load P_c of the type (A.3)

$$\gamma = \frac{V_o}{r} = 3 \left[\frac{P_y}{P_c} - 1\right] \left[1 - \sqrt[3]{\frac{P_c}{P_E}}\right] \tag{1.3}$$

where r is the relevant core radius of the section.

If the relationship between P_c and γ is known and γ is a random variable, it is conceptually easy to obtain the probability distribution of the dependent random variable P_c or $\sigma_c = P_c/A$. In Ref.(A.3), eq.(1.3) was assumed to hold throughout the relevant range; and, since the geometrical imperfection is essentially due to errors of fabrication with respect to the straight strut one aims at, it appeared logical to take γ to be normally distributed with zero mean, although only its absolute value, γ , appears in eq.(1.3). Fig.1.3 shows typical probability density curves of the collapse stress σ_c, calculated under the

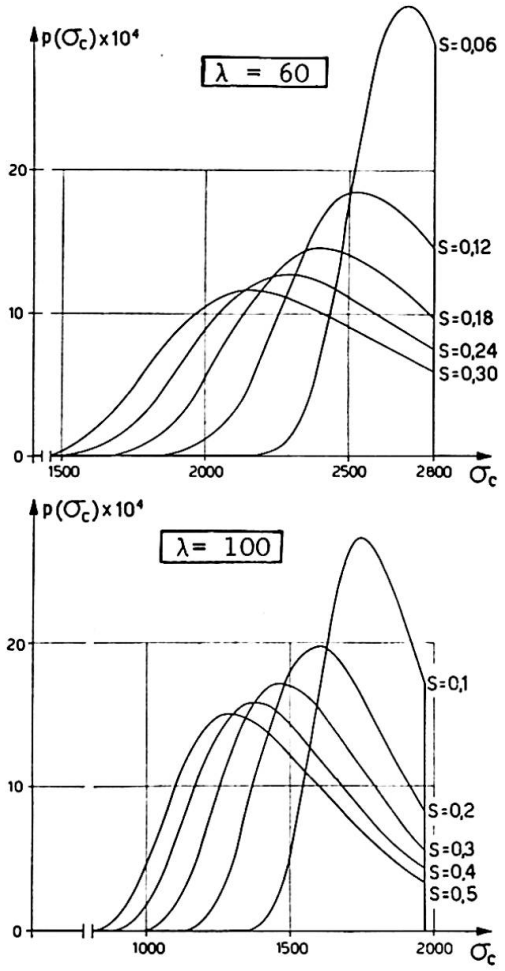

Fig. 1.3

above assumptions for the yield stress σ_y = 2800 kg/cm^2, two slenderness ratios λ, and several values of the standard variation, s, of the imperfection coefficient γ. All these curves show a sharp cut-off at the collapse stress of the imperfect strut

$$\sigma_{co} = P_{co}/A = \min(\sigma_y, \sigma_E): \quad \sigma_{co} = \sigma_y$$

when $\lambda = 60$, $\sigma_{co} = \sigma_E = P_E/A$ when $\lambda = 100$.

For a more realistic treatment, one must remember that the yield stress of a given material is also a random quantity : some earlier investigations seem to suggest that, at least in a first approximation, it can be considered to be normally distributed with a standard deviation, t, equal to about 10% of its mean value $\bar{\sigma}_y$. In the already quoted Ref. (A.3), it seemed appropriate to introduce also a random variability of the slenderness ratio λ, because this quantity may be different from the design value because of defective restraints and/or approximations introduced in the calculations; also λ has been assumed to be normally distributed, and its standard deviation, k, has been taken equal to 10% of the average value $\bar{\lambda}$. With these assumptions, the probability density curves of the collapse stress σ_c take the form shown in Fig. 1.4 : the upper cut-off disappears,

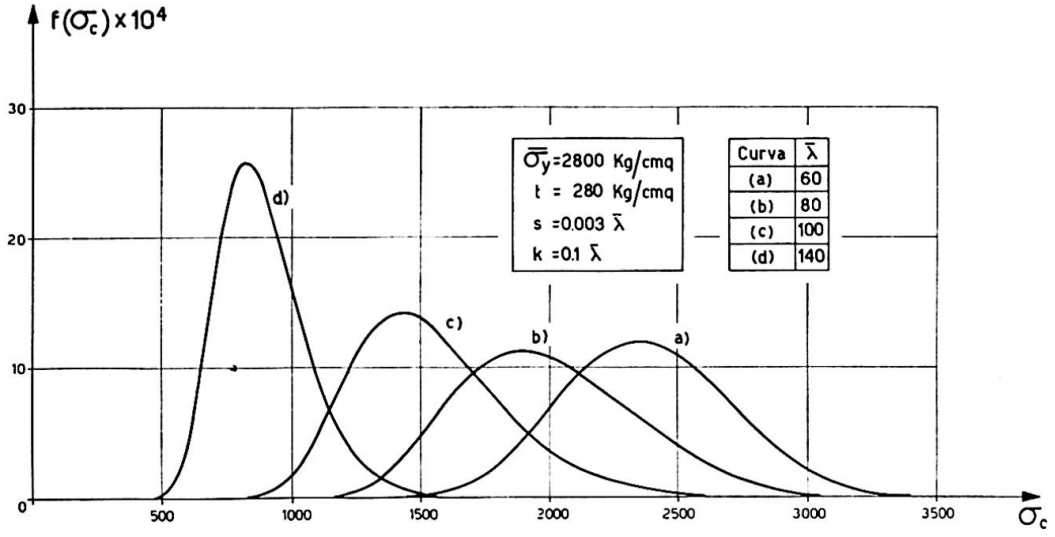

Fig. 1.4

because large values of σ_{co} are now possible, albeit with little probability. However, the average collapse stress $\bar{\sigma}_c$ remains much smaller than the collapse stress of the average, straight strut, $\sigma_{co} = \min(\bar{\sigma}_y, \bar{\sigma}_E)$.

In order to have indications for actual design practice, the relationship has also been investigated between the nominal safety factor ψ introduced in the calculations (ratio of nominal collapse stress σ_{co} to design admissible stress σ_{cam}) and the probability of collapse

$$P^* = \text{Prob}\ (\sigma_c \leq \sigma_{cam}) \tag{1.4}$$

A typical set of curves, plotted in semi-logarithmic scale in the relevant range of (very small) values of P^*, is shown in Fig. 1.5 : they can be well approximated by a set of parallel straight lines. It is also worth noting that very small variations of the nominal safety factor ψ can easily induce ten- or hundred-fold variations of actual safety; this clearly calls for a "rationalization" of design practice through the probabilistic approach. A qualitative and quantitative comparison between the results of the probabilistic treatment just summarized and the Italian Steel Building Code has also been presented in Ref. (A.3).

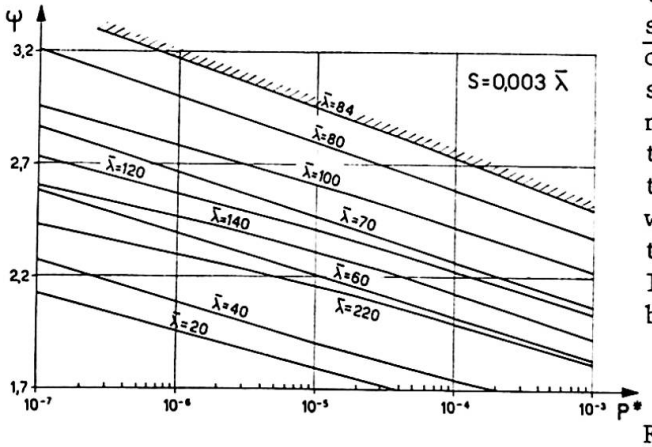

Fig. 1.5

2) ELASTIC BUCKLING: ASYMMETRIC BEHAVIOUR

The behaviour described in Section 1 is, within the elastic range, perfectly symmetrical with respect to the sign of the displacement and/or the imperfection, regardless of a possible asymmetry of the strut cross-section with respect to the axis of bending : in fact, the geometry of the section affects the behaviour of strut only through its moment of inertia. This type of behaviour (symmetric elastic buckling) is not limited exclusively to the pin-ended strut, but is common to many of the elastic structures that are liable to instability : indeed, before the development of Koiter's theory (Bieniek's Refs. 47 and 71), it was thought to be common to them all.

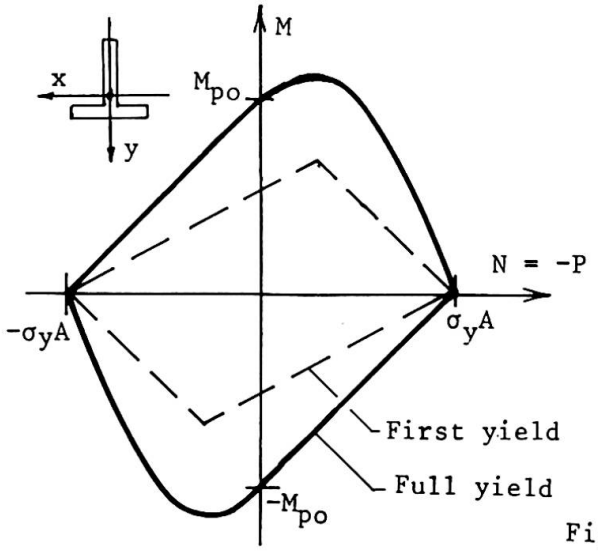

Fig. 2.1

However, the symmetry of behaviour does not extend beyond the elastic range of deformation, unless the strength of the cross-section is symmetric (as it has implicitly been assumed throughout Section 1). For instance, if the strut of Fig. 1.1 has a T-section, the first- and full-yield interaction curves in the moment-axial load (M-N) plane are qualitatively indicated in Fig. 2.1. (For a detailed derivation, cf. Ref. (A.5).)

Transformed into P–v coordinates, the interaction curves appear like in Fig. 2.2, and the P–v equilibrium paths become, on the whole, asymmetric for both

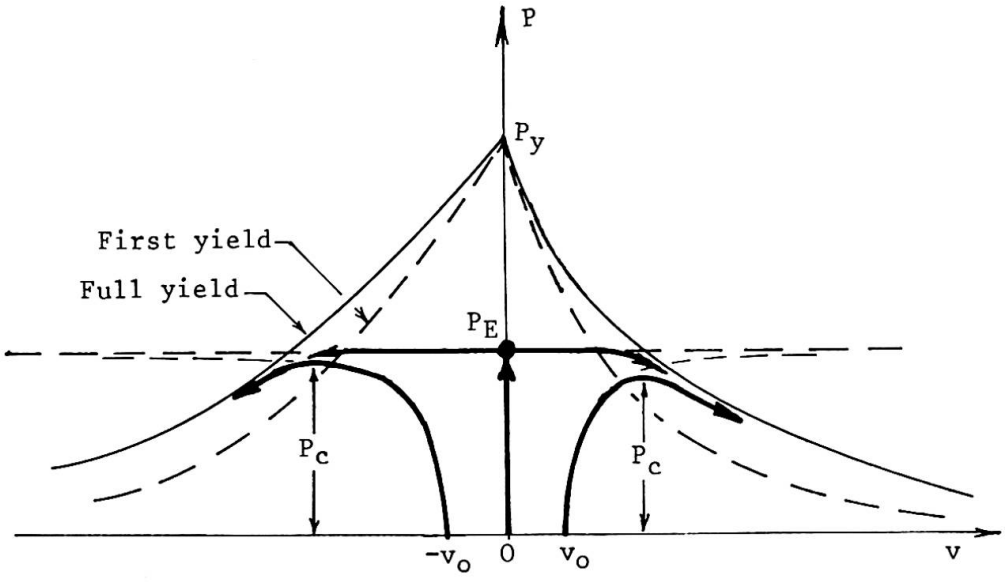

Fig. 2.2

the perfect and the imperfect strut, in both cases $P_E < P_y$ (illustrated by Fig. 2.2) and $P_y \leq P_E$ In particular, the collapse load does depend on the sign of the imperfection

$$P_c\,(V_o) \neq P_c\,(-V_o) \qquad (2.1)$$

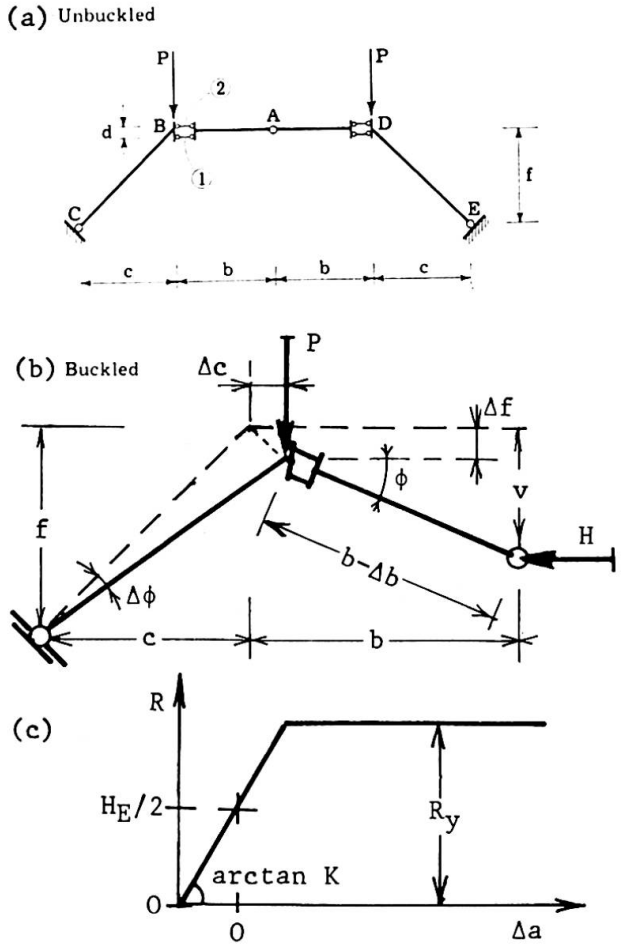

Fig. 2.3

The preceding discussion has illustrated the case of symmetric elastic buckling, followed by asymmetric plastic collapse due to an asymmetry of the cross-section : an asymmetry of yield stress (different yield points in tension and compression) would have the same qualitative effect.

Another important case of asymmetric behaviour is that of asymmetric elastic buckling, analytically described in the already quoted works by Koiter and here illustrated by the simple model of a three-hinged arch shown in Fig. 2.3a: AB, BC, etc. are rigid links; A, C, E are momentless hinges; the two deformable cells B and D consist of two parallel elastic rods (1 and 2) and a soft core that does not allow a shear deformation of the cell. Assume that Fig.2.3a represents the configuration at the point of buckling with a load $P = P_E$ and a horizontal thrust

$$H_E = P_E\, c/f \qquad (2.2)$$

The following treatment is limited to geometrically symmetrical buckled configurations, such as in Fig. 2.3b; equilibrium yields

$$\begin{aligned} P\ (c + \Delta c) &= H\ (f - v) \\ H\ (v - \Delta f) &= (R_1 - R_2)\ \frac{d}{2} \\ H &= R_1 + R_2 \end{aligned} \qquad (2.3)$$

where R_1 and R_2 are the (compressive) reactions in the elastic rods, related to their variation of length by (Fig. 2.3c)

$$K\ \Delta a_i = R_i - H_E/2 \qquad (i = 1,2) \qquad (2.4)$$

Δa_i is measured with respect to the point of buckling, and is taken positive when a shortening.

In deriving the post-buckling P-v relationship, introduce firstly the (wrong) assumption that the deformable cells do not change length during the deformation. Then geometry yields, up to second-order infinitesimals

$$(\phi - \Delta\phi)\ d = \Delta a_1 - \Delta a_2 \qquad (2.5)$$

$$\Delta c = b\ (1 - \cos\phi) = \frac{b\ \phi^2}{2} \quad ; \quad \Delta f = \frac{c}{f}\ \Delta c = \frac{bc}{f}\ \frac{\phi^2}{2} \qquad (2.6)$$

$$\phi = \frac{v - \Delta f}{b} = \frac{v}{b} - \frac{c}{f}\ \frac{\phi^2}{2} \quad ; \quad \Delta\phi = \frac{\Delta f}{c} = \frac{\Delta c}{f} = \frac{b}{f}\ \frac{\phi^2}{2} \qquad (2.7)$$

Introducing into eqs. (2.3), taking account of (2.4) and letting

$$P_E = H_E\ \frac{f}{c} = K\ \frac{d^2}{2b}\ \frac{f}{c} \qquad (2.8)$$

some algebra leads to the following expression

$$P = P_E\ (1 - \frac{3}{2}\ \frac{v}{f} + \ldots) \qquad (2.9)$$

Note that neglecting the second-order quantities $\Delta\phi$, Δc and Δf in the initial equations (2.3), the final equation would be

$$P = P_E\ (1 - \frac{v}{f}) \qquad (2.10)$$

i.e. would present an error of the same order of v : the possibility of such an error was pointed out by Koiter with reference to a simple fully elastic frame (A.6).

Actually, during buckling, the length of the elastic cells decreases of the quantity

$$\Delta b = (\Delta a_1 + \Delta a_2)\ /\ 2 \qquad (2.11)$$

Eqs. (2.6a) and (2.7b) become respectively

$$\Delta c = (b - \Delta b)\ (1 - \cos\phi) = b(\frac{\phi^2}{2} + \frac{\Delta b}{b}) \qquad (2.12)$$

$$\Delta\phi = \frac{\Delta c}{f} = \frac{b}{f}\ (\frac{\phi^2}{2} + \frac{\Delta b}{b})$$

Introducing these new expressions into (2.3) and (2.4) and rearranging, one obtains

$$2\,\phi\,\frac{\Delta b}{b} = -\frac{d^2}{2f}\left(\frac{\phi^2}{2} + \frac{\Delta b}{b}\right) \tag{2.13}$$

so that, up to second-order terms,

$$\frac{\Delta b}{b} = -\frac{\phi^2}{2} \quad ; \quad \Delta c = \Delta f = \Delta\phi = 0 \tag{2.14}$$

and eq. (2.10) holds, at least in the vicinity of the P-axis: this equation has been accepted in an earlier presentation of this arch model (A.7).

The limit condition of the arch corresponds to the most stressed rod reaching its yield value R_y (Fig.2.3c): the first- and full-yield M-N interaction profiles of the cells coincide into a diamond (Fig.2.4). Neglecting, in accord with eq. (2.14), all second-order displacements, it is easy to transform this diamond into the following P-v curves:

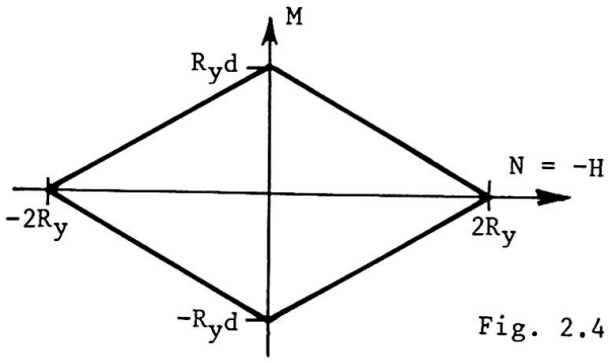

Fig. 2.4

$$v > 0;\ R_1 = R_y;\ P = P_y\,\frac{1-v/f}{1+2\,v/d} \tag{2.15}$$

$$v < 0;\ R_2 = R_y;\ P = P_y\,\frac{1-v/f}{1-2\,v/d} \tag{2.16}$$

where

$$P_y = 2\,R_y\,f/c \tag{2.17}$$

Eqs. (2.15) and (2.16), qualitatively sketched in Fig. 2.5, have the horizontal asymptote

$$P = \mp\,P_y\,d/2f \tag{2.18}$$

respectively; eq. (2.15) intersects the v-axis at v = f, with a slope

$$\left[\frac{dP}{dv}\right]_{P=0} = -\frac{P_y}{f}\,\frac{1}{1+2\,f/d} \tag{2.19}$$

so that, provided $P_y > P_E > P_y/(1+2\,f/d)$, eq.(2.10) intersects both eqs. (2.15) and (2.16) (Fig. 2.5). In words, elastic buckling of the perfect elastic arch just described is followed by compression yielding in the deformable cell.

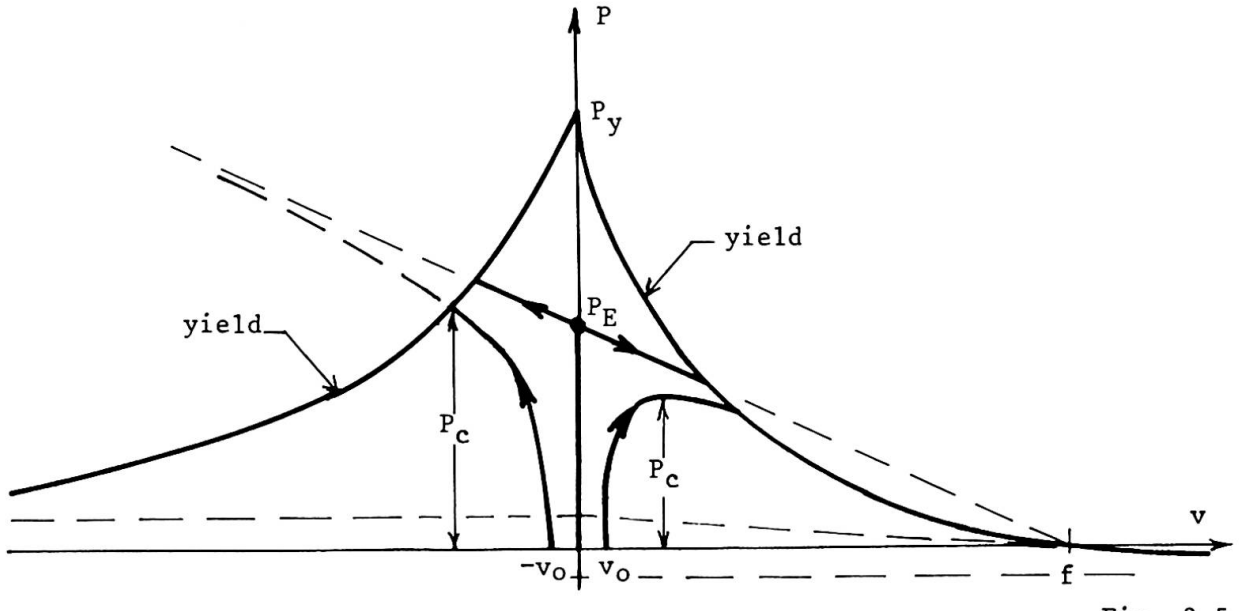

Fig. 2.5

If an initial imperfection, v_o, is present, the elastic P-v paths tend asymptotically to the straight line, eq. (2.10). Therefore, as shown in Fig. 2.5, when $v_o > 0$ the collapse load P_c is most probably reached within the elastic range of behaviour, while if $v_o < 0$ collapse occurs at the yield limit curve. It is thus shown that, in a structure liable to asymmetric elastic buckling, (a) the sign of the imperfection may affect the value of the collapse load as well as the qualitative type of collapse; and (b) the possibility of yielding may have no influence on collapse, if the imperfection weakens the structure.

3) STRUCTURES THAT BUCKLE IN THE INELASTIC RANGE

If the structural material is elastic-perfectly plastic, inelastic buckling occurs, under a rapidly decreasing load, when $P_y < P_E$, as in Fig.1.2b: the corresponding modifications of Figs. 2.2 and 2.5 are immediate. If the material has a non-zero inelastic modulus E_T, the simplest case of buckling beyond the elastic range is well illustrated by the well known Shanley's strut model (A.8). Assuming a constant modulus E_T and elastic unloading (Fig. 3.1),

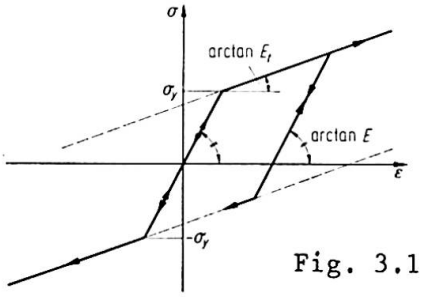

Fig. 3.1

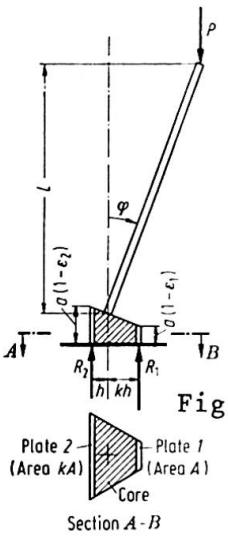

Fig. 3.3

Fig. 3.2

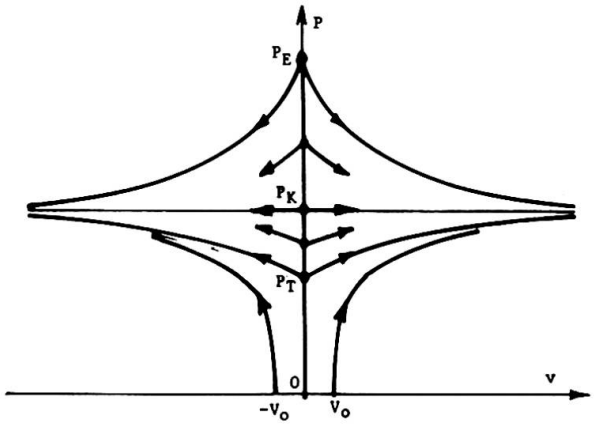

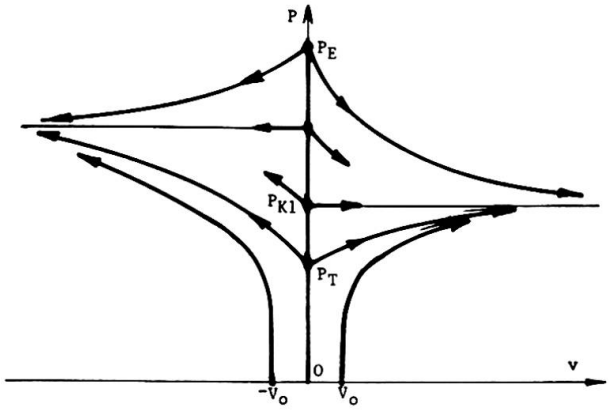

Fig. 3.4

the inelastic perfect strut may buckle at any load comprised between P_T and P_E; all P-v paths have a horizontal asymptote at a load $P = P_K \in (P_T, P_E)$, so that the load increases with $|v|$ (and the strut is stable,(A.1)) if buckling starts between P_T and P_K, decreases if buckling starts between P_K and P_E(°). The

(°) The validity of these statements is limited to comparatively small values of v. Otherwise, not only the small-displacements approximation loses validity, but the material may yield in tension in the "unloading" zone, or E_T may vary in the "loading" zone. Note that the latter probably occurs before the former in a real material, at least in the more significant range $P \leq P_K$, where the average stress $\sigma = P/A$ increases with the deformation.

loads P_T and P_K are obtained from the formula for the elastic buckling load P_E, substituting the elastic (Young's) modulus E, respectively with the tangent modulus E_T and with the so-called reduced modulus E_K, that depends on E, E_T and the shape of the section.

If the strut is not initially straight, the P-v path lies on either side of the P-axis according to the sign of the initial imperfection v_o, and below the lowest path of the perfect strut (which starts from $P = P_T$, Fig.3.2), to which path it tends when $v_o \to 0$. But some degree of imperfection is unavoidable in an actual structure; therefore, of the infinite theoretically possible buckling paths, only the lowest ones seem to be significant from an engineering point of view. Collapse of the inelastic strut, be it perfect or not, occurs with one of the phenomena mentioned in the footnote on the previous page; for detailed examples see e.g. Refs.(A.4) and (A.9) dealing respectively with Shanley's model and with the practically important case of mild steel columns with residual stresses.

In Shanley's treatment and in the above description, the strut cross-section is assumed to be symmetric with respect to the axis of bending: the whole picture in Fig.3.2 is also symmetric with respect to the P-axis. But if the cross-section is not symmetric (as in the example of Fig.3.3, Ref.(A.1)) the buckling interval of the perfect strut (P_T, P_E) remains unique, but each P-v path is different for $v > 0$ and $v < 0$, including the initial slope $[dP/dv]_{v=0}$ and the horizontal asymptote (Fig.3.4). In case of inelastic buckling, therefore, an asymmetry of strength implies asymmetric behaviour from the first stages of deformation. Again, the P-v path of any imperfect strut "is below the relevant lowest branch of the perfect strut ... and tends to such branch when the imperfection tends to zero" (A.1); the effects of an imperfection clearly depend on its sign.

The previous examples illustrate the inelastic behaviour of structures that, in the elastic range, exhibit symmetric buckling. The model arch of Fig.(2.3) was used in Ref.(A.7) to exemplify the inelastic behaviour of a structure liable to asymmetric elastic buckling; the effects of imperfections on this model have been investigated in detail by Batterman (A.10). Another simple model and a more realistic example have been presented by Hutchinson (A.11), with qualitatively similar results.

Referring to (A.9) and (A.10) for the analytical treatment (°), the behaviour of the perfect arch is summarized by Fig.3.5, and that of the imperfect arch by Fig.3.6 (reproduced from (A.10)).

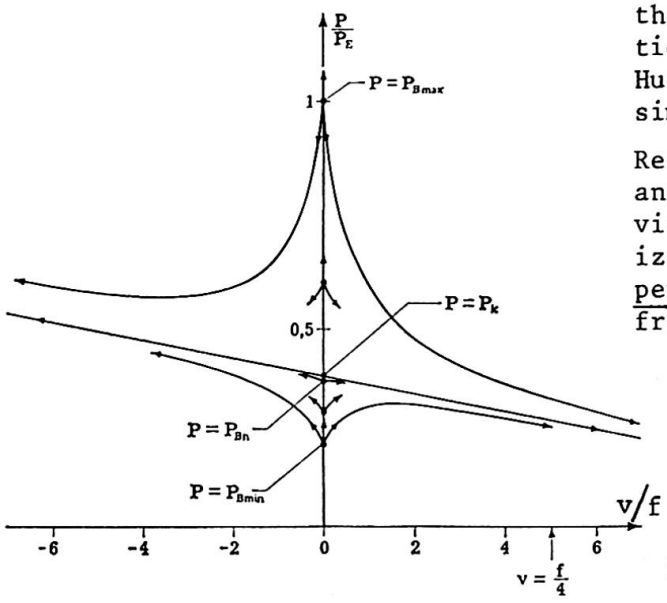

Fig. 3.5

(°) The second-order quantities Δc, Δf, etc., were neglected in the analysis (cf. eqs.(2.3) seqq.). This can be approximately justified, for small v, by the result of the complete elastic analysis, eqs.(2.14) and (2.10).

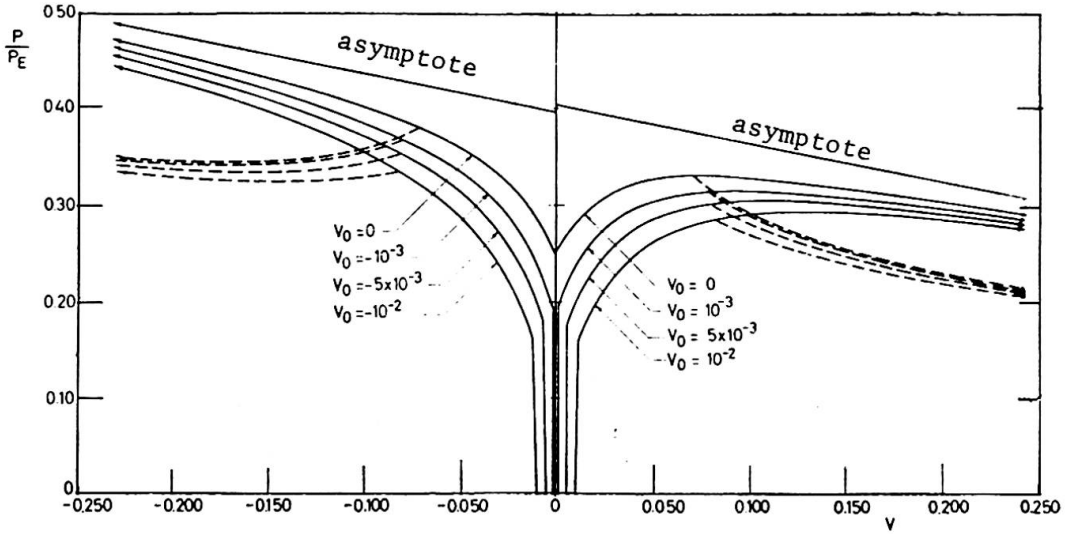

Fig. 3.6

Inspection of these Figures shows that the behaviour of the arch is markedly asymmetric, in the sense that it depends strongly on the sign of the displacement (and the initial imperfection). As in the previous examples, all paths of the imperfect structure ($v_o \neq 0$) lie below the lowest paths of the perfect one ($v_o = 0$) and tend to either of these when $v_o \to 0$ (Fig. 3.6); the straight asymptotes have a finite slope and, as noted by Batterman, are different on either side of the P-axis. The perfect arch is stable, for zero displacement, up to a load indicated by P_{Bn} in Fig. 3.5; but, when buckling with positive v, it always reaches a collapse point and becomes unstable. The imperfect arch collapses only (and always) when $v_o > 0$, unless account is taken of the possibility of tension yielding (which leads to the dashed lines of Fig.3.6) or of a decrease in E_T.

The behaviour illustrated by Figs. 3.5 and 3.6 is the inelastic analogue of Koiter's asymmetric elastic buckling.

REFERENCES

(A.1) G. Augusti, Instability of Continuous Systems (IUTAM Symposium Herrenalb 1969, edited by H. Leipholz), pp.175-182; Springer, Berlin 1971.
(A.2) G. Augusti and A. Baratta, Journ.Structural Mechanics, 1, No.1, 1972.
(A.3) G. Augusti and A. Baratta, Costruzioni Metalliche, 23, No.1, 1971 (in Italian) and Construction Metallique, 8, No.2, 1971 (in French).
(A.4) G. Augusti, Ingegneria Civile, No.11, 1964.
(A.5) J. Baker and J. Heyman, Plastic Design of Frames, Vol.I, pp.25-28; Cambridge Univ. Press 1969.
(A.6) W.T. Koiter, Recent Progress in Applied Mechanics (The Folke Odqvist Volume); pp.337-354; Almqvist & Wiksell, Stockholm 1967.
(A.7) G. Augusti, Meccanica (AIMETA), 3, No.2, 1968.
(A.8) F.R. Shanley, J.Aero.Sci., 14, No.5, 1947.
(A.9) G. Augusti, Journ.Engrg.Mech.Div., ASCE, 91, No.EM4, 1965.
(A.10) S.C. Batterman, Israel J. Technology, 9, No.5, 1971.
(A.11) J.W. Hutchinson, Conference on Computer-Oriented Analysis of Shell Structures, Palo Alto, California, 1970.

SUMMARY

The influence of random imperfections and inelastic deformations on the buckling and post-buckling behaviour of structures has been examined in several cases.

The financial support of the Italian National Research Council (CNR) is acknowledged.

Leere Seite
Blank page
Page vide

Interaction of Postcritical Plate Buckling with Overall Column Buckling of Thin-Walled Members

Interaction du voilement post-critique de plaques et du flambement de colonnes aux parois minces

Wechselwirkung von überkritischem Plattenbeulen und Knicken des ganzen dünnwandigen Stabes

JOHN DeWOLF TEOMAN PEKOZ GEORGE WINTER
Cornell University, Ithaca, New York, USA

I. Introduction

The interaction of postcritical plate buckling with overall column buckling in thin-walled members is a complex phenomenon which is very important in many situations. Thin-walled steel construction in buildings has increased greatly in the past two to three decades; thin-walled members have always been used extensively in aircraft construction.

In thin-walled members plate buckling is of major importance and constitutes one of the chief design criteria. The classical critical plate buckling stress for the component plates, which is the stress at which local bifurcation buckling occurs, is often regarded as the chief design criterion. However, this is by no means the maximum load which the component plate can carry. The plate will usually continue to take increasing load, often more than twice the critical local buckling load. This postcritical plate buckling strength can be used to achieve substantial economies.

This paper concerns itself with postcritical plate buckling and its effect on the overall buckling of columns. For most thin-walled columns of low and medium slenderness, critical plate buckling of one or more of the component plates occurs first, and is then followed by overall column buckling at some point in the postcritical plate buckling range. The prior plate buckling lowers the overall capacity of the column, but the load at which local bifurcation buckling occurs is less than the actual carrying capacity of the member and may not be used as a reasonable indication of the overall capacity.

The investigation reported herein has been sponsored at Cornell University by the American Iron and Steel Institute. It is aimed at developing information on this interaction between postcritical plate buckling and overall column buckling. Thirty-three tests have been conducted on columns in which both the postcritical plate buckling strength and the overall column buckling strength were varied systematically. The results of these tests illustrate clearly the interaction effects between postcritical plate buckling and overall

column buckling.

II. Survey of Previous Work

Many researchers have investigated plate buckling and a number have done work in the postcritical plate buckling range; also, overall column buckling has been extensively investigated. However, little has been done in the area of the interaction of postcritical plate buckling with overall column buckling. In fact, postcritical plate buckling by itself needs further clarification. This refers particularly to the later stages, where relatively large plate deflections interact with nonlinear materials' behavior.

One researcher, T.R.G. Smith in England[1], has made a very important contribution in the field which considers both of the above nonlinearities in the postcritical plate buckling range as they interact with overall column buckling. Unfortunately his analysis is limited to tubes and cannot be applied to other shapes without repeating his lengthy derivations for each type of section.

Some work has been done toward a simpler method of treating different types of common sections such as by Uribe [2] and Wang [3] at Cornell University, though their work was primarily involved with things other than interaction effects and was not very extensive. Others [4-7] have made contributions to the field of interaction, but their work has not involved both types of nonlinearities as has T.R.G. Smith. There appears to be no thorough set of tests utilizing different column shapes upon which a general method of design of thin-walled columns subject to the interaction of postcritical plate buckling with overall column buckling can be based.

III. Testing

Since thin-walled members are made of essentially two types of elements, elements with one edge stiffened by a web, flange or stiffener and elements with both edges stiffened, two types of sections were chosen in order to test each type of element separately. One section was composed entirely of stiffened elements; it was made of two channels connected together at the flanges to form a rectangular tube (see Fig. 1a). The other was composed primarily of unstiffened elements (the stiffened element was designed so that local buckling would not occur); it was made of two channels connected back to back along the webs to form an "H" type section (see Fig. 1b).

Four sections of each type were fabricated. The dimensions of the sections were chosen so that the critical and postcritical plate buckling strength were varied by varying the element width-thickness ratios over a wide range. The dimensions are given in Table 1.

For each section, the overall column buckling strength was varied by varying the slenderness ratio L/r. In addition to a stub column test (no column buckling), three different column lengths were chosen to cover the region in which local buckling had an effect on the ultimate load a column will support.

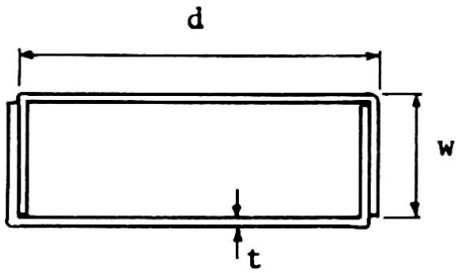

(a) Section S

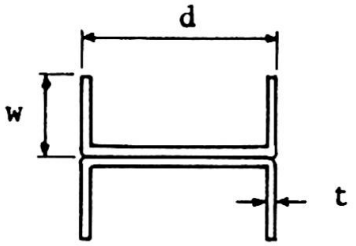

(b) Section U

Fig. 1 Column Cross-Sections

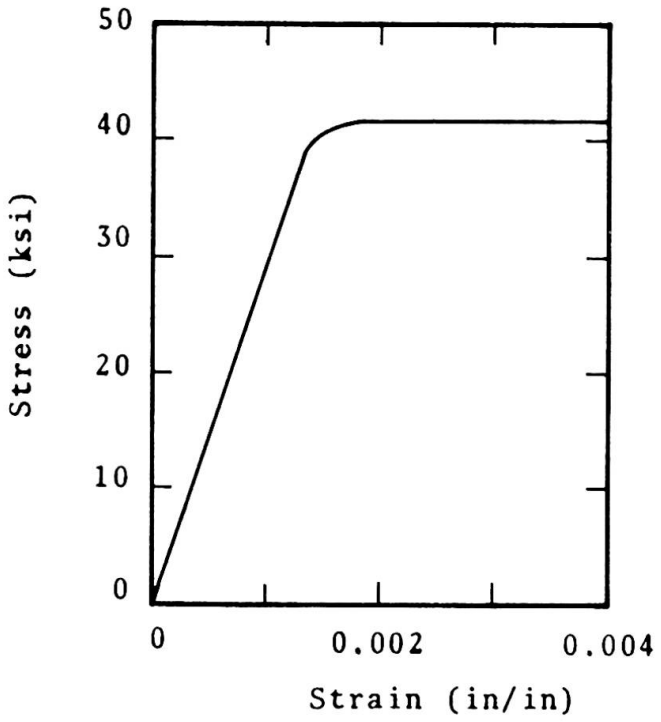

Fig. 2 Material Stress-Strain Curve

The testing arrangement was such that concentric loads were achieved. This was done by loading to approximately twenty percent of the expected failure load and then unloading and making adjustments in the centering as necessary. Dial gages were used to measure the lateral deflections and strain gages to obtain the strain distributions, as well as to determine approximately when local buckling occurred in the plate elements. It is easily verified from the strain gage results that nearly concentric loads were achieved in all of the columns, except for three tests which were eccentric and whose results are ignored.

Measurements of the out-of-plane deflections were taken for all of the unstiffened plate elements. It was found that these deflections were minimal until failure, being no more than a few thousandths of an inch.

The initial portion of the stress-strain curve for the material used, a carbon steel of a structural quality, is shown in Fig. 2. The average yield stress was 41.9 ksi., and the average ultimate stress was 53.8 ksi. Strain hardening occurred at an average strain of 0.014. The average percentage of elongation of a two-inch gage length at rupture was 37 percent.

IV. Results

(a) General

The results of these tests illustrate clearly the interaction between postcritical plate buckling behavior and overall column

Table 1

DIMENSIONS OF SECTIONS

(a) Sections S

Specimen	w (in)	d (in)	t (in)	Width/Thickness Single Thickness Element (d/t)	Width/Thickness Double Thickness Element (w/2t)
S-1	2.0	3.5	0.058	57.2	16.7
S-2	2.0	5.0	0.058	83.0	16.7
S-3	2.0	7.0	0.058	117.4	16.7
S-4	2.0	9.0	0.058	151.8	16.7

(b) Sections U

Specimen	w (in)	d (in)	t (in)	Width/Thickness Single Thickness Element (w/t)	Width/Thickness Double Thickness Element (d/2t)
U-1	1.0	3.0	0.058	16.2	24.8
U-2	1.25	3.0	0.058	20.5	24.8
U-3	1.5	3.0	0.058	24.8	24.8
U-4	1.75	3.0	0.058	29.1	24.8

buckling. The ultimate carrying capacities for the columns are given graphically in Figs. 3 and 4. The figures compare the experimental carrying capacity with the expected strength (1) when local instability is entirely neglected; (2) when the effect of local instability is based on the critical bifurcation stress, neglecting postcritical strength; (3) when postcritical buckling is included approximately by means of an effective width concept. These will now be discussed separately.

(b) Local Instability Neglected

A concentric, perfect column which is elastic will fail at the critical Euler stress or at the yield stress, provided that local instability and residual or cold-forming effects are nonexistent. For this type of column behavior, column curves, i.e. slenderness ratio vs. critical stress, are given as curves (1) in Figs. 3 and 4 for each of the different sections.

As mentioned, this neglects the effects of local instability, which were present in the test specimens. Additionally, the specimens were cold-worked so that cold-forming effects were present. However, since cold-forming effects are related to the area of the corners as a fraction of the total area (8), and since the ratio of the corners to the total area was less than one percent for all of the sections, the cold-forming effects were negligible. The columns

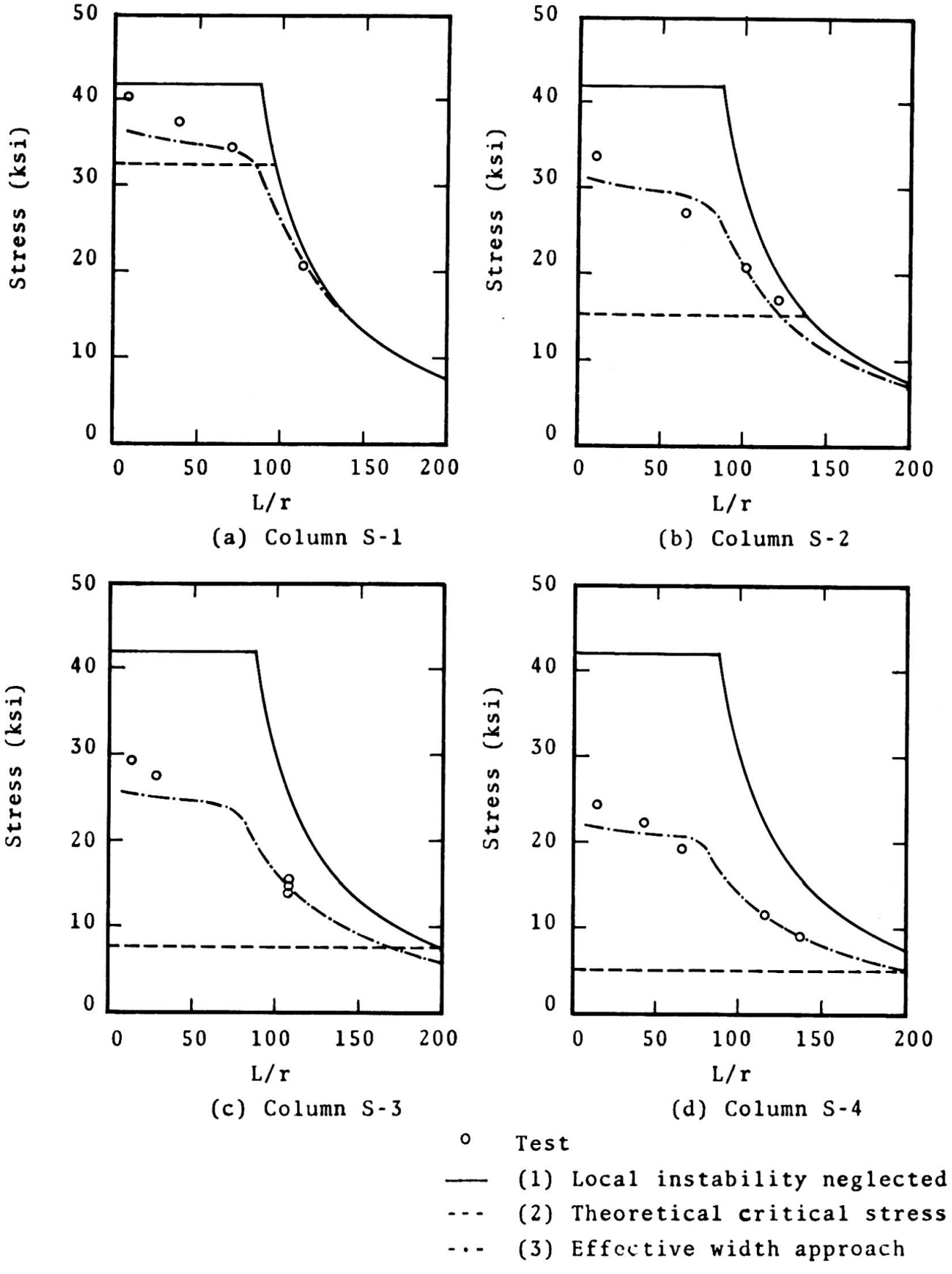

Fig. 3 Comparison of Test Results and Column Curves For Column Specimens S

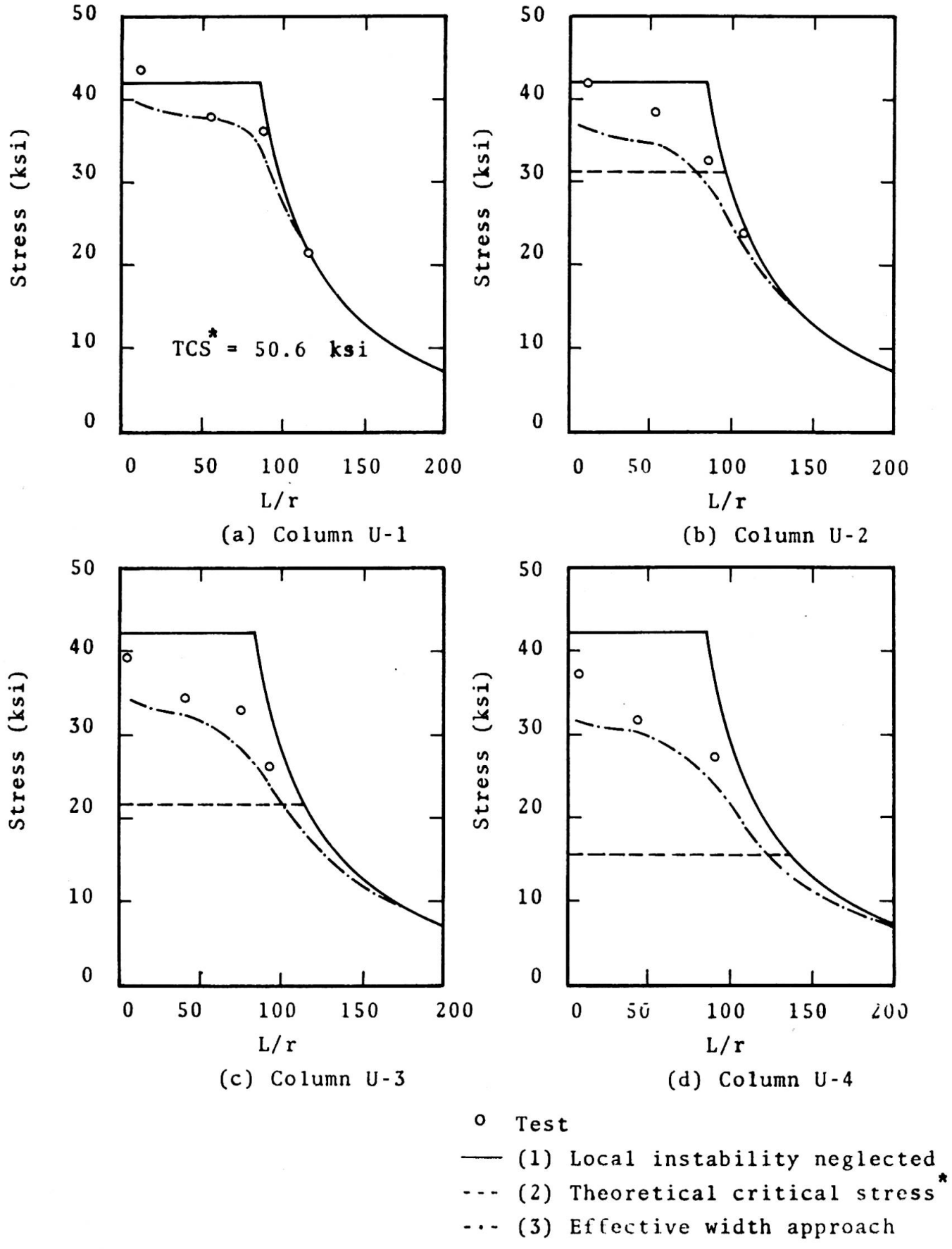

Fig. 4 Comparison of Test Results and Column Curves For Column Specimens U

were thus assumed to have a uniform stress-strain curve which is approximated by the material stress-strain curve in Fig. 2.

It is seen that almost all test points fall significantly below curves (1) which indicates that local instability had a great effect on strength. This effect became greater as the width/thickness ratios of the elements were increased.

(c) Theoretical Critical Stress

The theoretical critical bifurcation stress is that stress at which a perfect plate begins to buckle. Here it refers to the widest elements for the closed tubular sections and to the unstiffened flanges for the "H" sections. The theoretical critical stress by definition is the stress at which postcritical strength begins.

The classical critical stress for a plate element that buckles elastically is calculated from:

$$\sigma_{cr} = k \frac{\pi^2 E}{12(1 - \mu^2)(\frac{w}{t})^2} \qquad 1$$

where E is the modulus of elasticity, μ Poisson's ratio, w the plate width, t the plate thickness, and k depends on the edge conditions, chiefly along the longitudinal edges parallel to the compression stress. Values of k which are often used in practice, and which in some cases will be conservative, are 0.5 for elements with one edge supported by a web and the other edge unsupported, and 4.0 for elements with both edges supported by a web.

For the purpose of comparing the test results to a theoretical stress, these two values of k were used for the sections under study. The results are given in curve (2) in Figs. 3 and 4. With the exception of Fig. 4a the theoretical critical stress was below the highest load at failure, indicating that postbuckling strength existed. For Fig. 4a, the theoretical elastic critical stress was above the yield stress, though the section showed local waving prior to failure during the tests. It is seen that, except for Fig. 4a, almost all test points fall significantly above curve (2) indicating that postcritical strength does add considerably to the carrying capacity. This effect increases with increasing width/thickness ratios.

(d) Effective Width Approach

In order to consider the postbuckling strength, an effective width approach is now under development. At present, this approach is only an approximate method for considering postbuckling strength, and in its present form is not always satisfactorily accurate. The concepts of the method are these:

The bifurcation stress of a column is well accepted to be given by the Engesser-Shanley tangent-modulus equation:

$$\sigma_t = \frac{\pi^2 E_t}{(\frac{KL}{r})^2} \qquad 2$$

where E_t is the tangent modulus for the material, L is the column length, r is the radius of gyration, and K is the effective length factor. Dividing the cross-section into j elements, one can define:

$$E_t r^2 = \frac{\sum_{i=1}^{j} E_{ti} I_i}{A} \qquad 3$$

Then, for K = 1.0, by substitution, Eq. 2 becomes:

$$L^2 = \frac{\pi^2 \sum_{i=1}^{j} E_{ti} I_i}{\sigma A} \qquad 4$$

where, for any selected strain, E_{ti} is the tangent modulus of the i^{th} element, I_i is the moment of inertia of the i^{th} element about the weak principal axis, A is the full area of the cross-section, and σ_{cr} is given by:

$$\sigma = \frac{\sum (A_{eff})_i \sigma_i}{A} \qquad 5$$

where $(A_{eff})_i$ is the effective area of the i^{th} sub-element at the stress σ_i corresponding to the assumed strain ε, and A is the full area of the section. Essentially, Eq. 5 considers the effects of local buckling and postbuckling strength by reducing the area to an effective area, using the effective widths of the elements.

The general equation for the effective width on which American specifications are now based is:

$$\frac{b}{w} = \sqrt{\frac{\sigma_{cr}}{\sigma_{max}}} \left(1 - 0.22 \sqrt{\frac{\sigma_{cr}}{\sigma_{max}}}\right) \qquad 6$$

which constitutes a slight revision of the equation first given by Winter [9]. Here b is the effective width, w is the real width of the particular plate element, σ_{cr} is the classical plate bifurcation buckling stress for the given edge conditions, and σ_{max} the edge stress in the postbuckling range. This equation can be transformed into the more convenient form:

$$b = C_1 t \sqrt{\frac{E}{\sigma_{max}}} \left(1.0 - C_2 \frac{t}{w} \sqrt{\frac{E}{\sigma_{max}}}\right) \qquad 7$$

where t is the plate element thickness, E the modulus of elasticity, and C_1 and C_2 are constants which depend on the edge conditions. For elements with one side supported by a web and the other side unsupported, approximately $C_1 = 0.672$ and $C_2 = 0.148$. For elements with both edges supported, approximately $C_1 = 1.9$ and $C_2 = 0.415$.

The ultimate loads predicted using this effective width approach

are given in curves (3) in Figs. 3 and 4. It is seen that the test results agree best with the last of the three methods (curve 3), which includes the effect of postcritical plate buckling strength on column capacity. At the same time, it is also seen that the accuracy of this approach is inadequate. Further development of this method is needed, and is under way at the present time.

V. Conclusions

On the basis of extensive test results and theoretical comparisons, it is shown that:

(1) The strength of thin-walled columns can be considerably reduced by local plate buckling.

(2) Column capacities calculated on the basis of the classical critical plate buckling stress considerably underestimate the actual column strength.

(3) The effect of the postcritical strength of the component plates increases the column strength significantly over that determined by the critical plate buckling stress.

(4) A tentative method, based on the postcritical effective width of plates, is now under development and promises to furnish a satisfactory tool for calculating the strength of thin-walled columns.

References

1. Smith, T.R.G., "The Ultimate Strength of Locally Buckled Columns of Arbitrary Length," Ph.D. Thesis, Cambridge University, 1966.

2. Uribe, J., "Aspects of the Effects of Cold-Forming on the Properties and Performance of Light-Gage Structural Members," Department of Structural Engineering, Report No. 333, Cornell University, May 1969.

3. Wang, S.T., "Cold-Rolled Austenitic Stainless Steel: Materials Properties and Structural Performance," Department of Structural Engineering, Report No. 334, Cornell University, July 1969.

4. Bijlaard, P.P., and Fisher, G.P., "Interaction of Column and Local Buckling in Compression Members," NACA T.N. 2640, 1952.

5. Bijlaard, P.P. and Fisher, G.P., "Column Strength of H-Sections and Square Tubes in the Post-Buckling Range of the Component Plates," NACA T.N. 2994, 1953.

6. Klöppel, K., and Schubert, J., "Die Berechnung der Traglast mittig und aussermittig gedrückter, dünnwandiger Stützen mit kastenförmigem Querschnitt in überkritischen Bereich," Veröffentlichung des Institutes für Statik und Stahlbau der Technischen Hochschule Darmstadt, Darmstadt, 1971.

7. Skaloud, M., and Zörnerová, M., "Experimental Investigation into the Interaction of the Buckling of Compressed Thin-Walled Columns with Buckling of their Plate Elements," ACTA Technica CSAV, No. 4, 1970, pp. 389-424.

8. Karren, K.W., "Effects of Cold-Forming on Light-Gage Steel Members," Department of Structural Engineering, Report No. 318, Cornell University, June 1965.

9. Winter, G., "Light-Gage (Thin-Walled) Steel Structures for Buildings in the United States of America," Int. Assoc. Bridge and Structural Engineering, Fourth Congress, Prel. Publ., 1952, pp. 523-538.

Summary

Experimental data are given which illustrate clearly the interaction of postcritical plate buckling with overall column buckling in thin-walled members. The experimental carrying capacity is compared with the expected strength when (1) local instability is entirely neglected; (2) the effect of local instability is based on the critical bifurcation stress, neglecting postcritical strength; (3) postcritical buckling is included approximately by means of an effective width concept.

Post-Buckled Behaviour and Incremental Collapse of Webs Subjected to Concentrated Loads

Comportement post-critique de voilement et ruine des âmes soumises à des charges concentrées

Überkritisches Beulverhalten und zusätzlicher Kollaps von Stahlblechen infolge konzentrierter Lasten

MIROSLAV ŠKALOUD
Docent, Ing., Dr.Sc.
Senior Research Fellow
at the Institute of Theoretical
and Applied Mechanics of the
Czechoslovak Academy of Sciences
in Prague, CSSR

PAVEL NOVÁK
Docent, Ing., CSc.
Research Fellow
at the Structural Institute
in Prague, CSSR

1. Introductory Remarks

After the completion of the investigation into the post-buckled behaviour of webs in shear, which was conducted partially by K.C.Rockey and the first of the authors in Swansea and Cardiff /1/ and partly, after the return of the author to Czechoslovakia, at the Institute of Theoretical and Applied Mechanics in Prague /2/, a new research project was started. This deals with the influence of flange stiffness upon the ultimate load behaviour and incremental collapse of thin webs subjected to a concentrated (or, more accurately, to a narrow partial edge) load. The investigation is carried out by a research team that consists of the first of the authors, Ing.Drdácký, Ing.Kratěna, Ing.Zörnerová (all of them from the Institute of Theoretical and Applied Mechanics in Prague), the other author and Ing.Bohdanecký (both from the Structural Institute in Prague). The objective is to obtain (together with other investigators /3/, /4/, /5/) enough information about the ultimate load behaviour of plate girders the webs of which are subjected to a patch load, such as are crane run-way girders, certain types of bridge girders and similar structures.

2. Test Girders

Two series of test girders were tested. The general details of the test girders of the first series are given in Fig. 1a, the corresponding dimensions (in mm) in Table 1a. The details of the second series girders are shown in Fig. 1b, and the dimensions in Table 1b.

An inspection of the figures shows that the test girders of the second series had two web panels. Each of them was tested individually, the supports being positioned under the boundary vertical stiffeners of the panel. Web panel W 2 was tested first, the girder being subjected to a static load.

Table 1a

Girder	Loading	Web			Flange						P_{cr}^{RB}	P_{ult}
		Depth b [mm]	Thickness t [mm]	$\frac{b}{t}$	Width b_f [mm]		Thickness t_f [mm]		I_f/a^3t [Units of 10^{-6}]			
					Upper	Lower	Upper	Lower	Upper	Lower	[T]	[T]
PT6 1	static	500	2	250	50	50	5.95	5.95	3.48	3.48	2.18	3.6
PT6 2	static						5.97	5.93	3.50	3.43	2.2	4.0
PT6 3	cyclic						5.09	5.03	2.17	2.09	2.38	5.0
PT6 4	cyclic						5.08	5.06	2.16	2.13	2.19	4.6
PT6 5	static				45	45	16.21	16.14	63.89	63.07	2.53	5.5
PT6 6	cyclic						16.24	16.14	64.25	63.04	2.53	5.5
PT6 7	cyclic						16.17	16.07	63.48	62.31	2.52	5.6
PT6 8	static						16.25	16.11	64.36	62.72	2.53	5.5
PT6 9	cyclic				50	50	24.25	24.78	237.68	253.60	2.83	7.2
PT610	cyclic						24.64	24.24	249.33	237.38	2.83	7.0
PT611	static						24.80	24.84	254.22	255.45	2.84	7.5
PT612	static						24.40	25.00	242.11	260.42	2.85	8.0

Table 1b

Girder	Web	Loading	Web			Flange						P_{cr}^{RB}	P_{ult}
			Depth b [mm]	Thickness t [mm]	$\frac{b}{t}$	Width b_f [mm]		Thickness t_f [mm]		I_f/a^3t [Units of 10^{-6}]			
						Upper	Lower	Upper	Lower	Upper	Lower	[T]	[T]
T6 1	W1	cyclic	1000	2.5	400	160	160	5.50	5.18	0.887	0.741	2.2	6.5
	W2	static											5.0
T6 1'	W1	cyclic						5.42	5.56	0.849	0.917		
	W2	static											
T6 2	W1	cyclic				200	200	10.09	10.08	6.85	6.83	2.24	7.0
	W2	static											6.5
T6 3	W1	cyclic						16.24	16.15	28.55	28.08	2.36	9.2
	W2	static											7.0
T6 4	W1	cyclic						20.17	20.12	54.70	54.30	2.48	9.8
	W2	static											9.0
T6 5	W1	cyclic				250	250	30.88	30.44	245.39	235.05	2.78	18.0
	W2	static											18.0
T6 5'	W1	cyclic						30.50	30.48	236.44	236.00		
	W2	static											

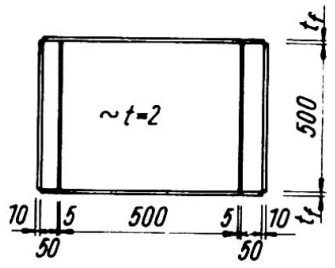

Fig. 1a

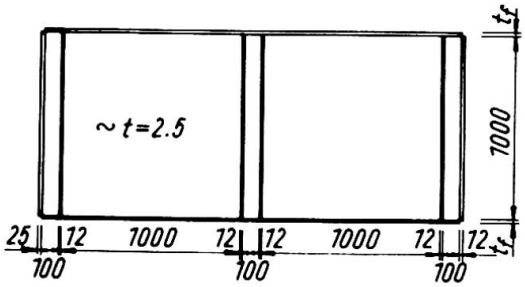

Fig. 1b

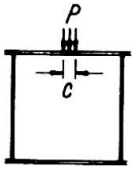

Fig. 2

Then this web panel was cut off, and web panel W 1 was subjected to a cyclic load.

All web panels in both aforesaid series had aspect ratio α of 1. Test girders with other α -ratios will be tested in 1972. In each series the depth-to-thickness ratio $\lambda = b/t$ of the web was constant, but the flange dimensions varied from girder to girder, so that the effect of the flexural rigidity of flanges upon the ultimate load behaviour of webs could be studied.

The research on steel girders was accompanied by a photoelasticity investigation conducted by the first of the authors and J.Kratěna on reduced-scale epoxy-resin models.

In all tests the web panels were subjected to a narrow partial edge load, applied on to the upper flange at the mid-distance of the vertical stiffeners. The width of the load c = a/10 (in one case c = a/5), a denoting the width of the web panel (Fig.2).

3. Apparatus

A description of the experimental apparatus and of the programme of measurements was the objective of the paper /6/ presented by the authors at the Congress of RILEM in Buenos Aires. For this reason only a brief information about the apparatus will be given in this publication, the aim of which is to discuss main test results.

The buckled pattern of the web was measured by means of a stereophotogrammetric method /7/. The application of this method was advantageous in the aforesaid tests, since it enabled the authors to take all readings in a very short time moment (0,001 sec.). This was desirable in the static load tests (because a study of the final, plastic, stage - in which the web and flanges were already yielding - was one of the main objectives of the investigation) and indispensable in the cyclic load tests (in which the web and flanges were "breathing").

A special device, designed by P.Pašník, enabled the authors to take deflection readings at a given moment of loading cycles; for example, when, in a "breathing" cycle, the web deflection attained its maximum (amplitude) value. Moreover, the stereophotogrammetric method made it possible to measure not only the deflection perpendicular to the web, but also the in-plane distortion of the mesh that was marked on the web, and the deformation of the boundary frame of the web panel.

A set of strain gauges was attached to both sides of the web and of the upper flange in order the stress pattern in the girder could be studied. Several of the strain gauges, as well as two deflection pick-ups, were linked to an automatic recorder "Ultralette". Thus it was possible to study, as a function of time, the progression of the plastification of the girder in the static load tests and the deflection (and strain) stability in the cyclic load ones.

The post-failure plastic residue in the web and flanges of each test girder was also carefully measured.

4. Static Load Tests

The first part of the investigation was concerned with the post-buckled behaviour of webs subjected to a static patch load. The influence of the flexural rigidity of flanges upon the buckled pattern and stress state in the web and flanges, and upon the ultimate load of the whole girder was studied.

The post-failure plastic residues w_{pl} in web panels W 2 of test girders TG 1 (flexible flanges) and TG 5 (rigid flanges) are plotted in Figs. 3a and b. The plastic residues in the upper (i.e. loaded) flange of girders TG 1, TG 3 and TG 5 are given in Fig. 3c. A photo of the collapsed girder TG 4 is shown in Fig. 3d.

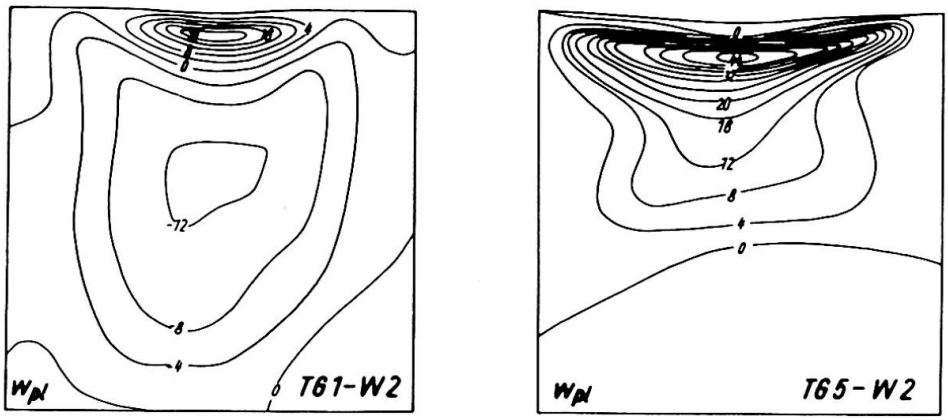

Fig.3

An inspection of the aforesaid figures shows the pronounced influence that flange stiffness has on the deformation of the test girder. While, in the case of flexible flanges, the buckling of the web and the deflection of the flanges are localized in the neighbourhood of the partial edge load, for heavy flanges the buckled pattern of the web and the flexure of the flange are distributed almost over the whole width of the web panel. The performance of the web panel is then more homogeneous; this affecting - as it will be demonstrated below - very beneficially the ultimate load behaviour of the girder.

The pattern of ε_{my} (ε_{my} denoting the vertical - i.e. parallel to the load - membrane strain) in web W 2 of girder TG 1 (flexible flanges) is given in Fig. 4. Fig. 4a shows the values of ε_{my} along two horizontal lines (the first of them being situated 30 mm and the other 300 mm from the top flange), and Fig. 4b gives the strains ε_{my} along the vertical axis of the web. The bending strains ε_{bx} in the upper (i.e. loaded)

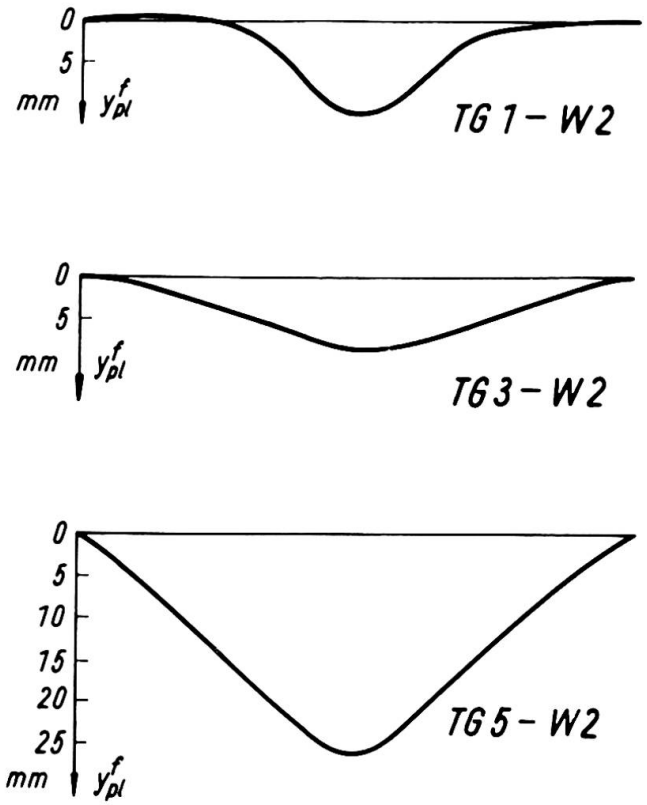
0
5
mm
y^f_{pl}
TG 1 – W2
0
5
mm
y^f_{pl}
TG 3 – W2
0
5
10
15
20
25
mm
y^f_{pl}
TG 5 – W2

Fig. 3c

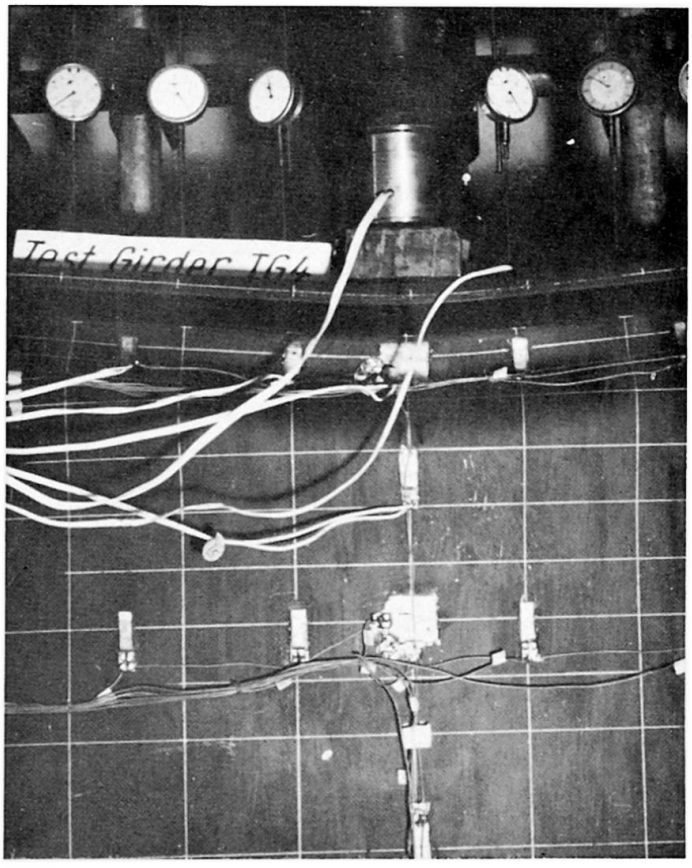
Test Girder TG4

Fig. 3d

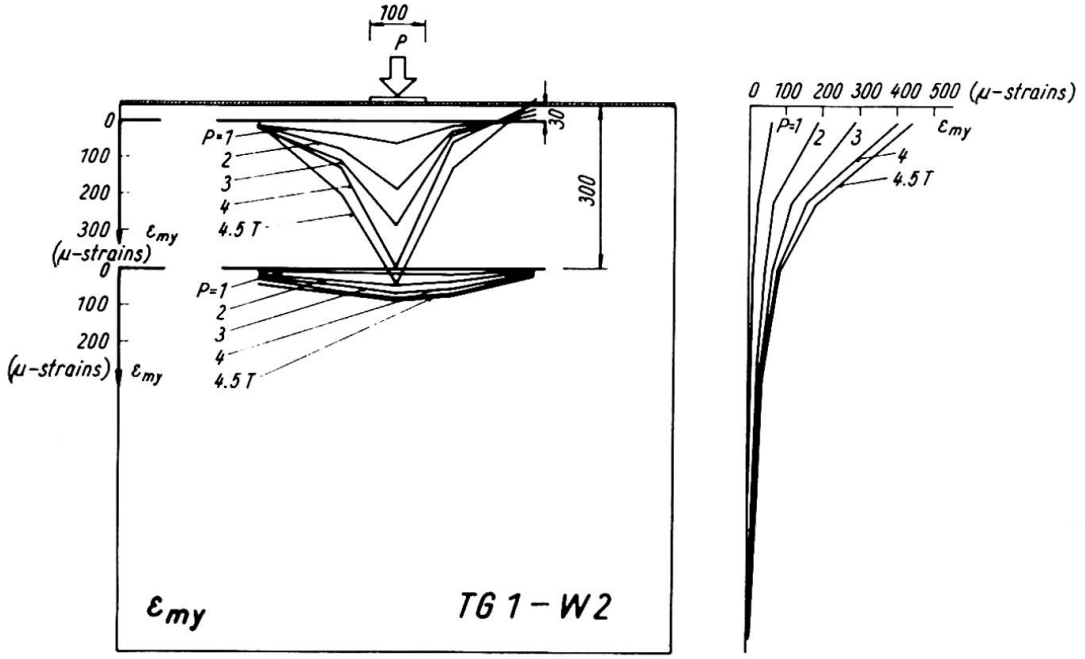

Fig. 4

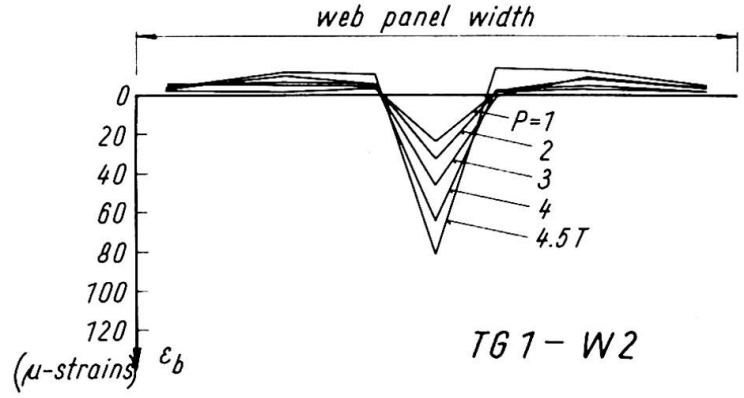

Fig. 5

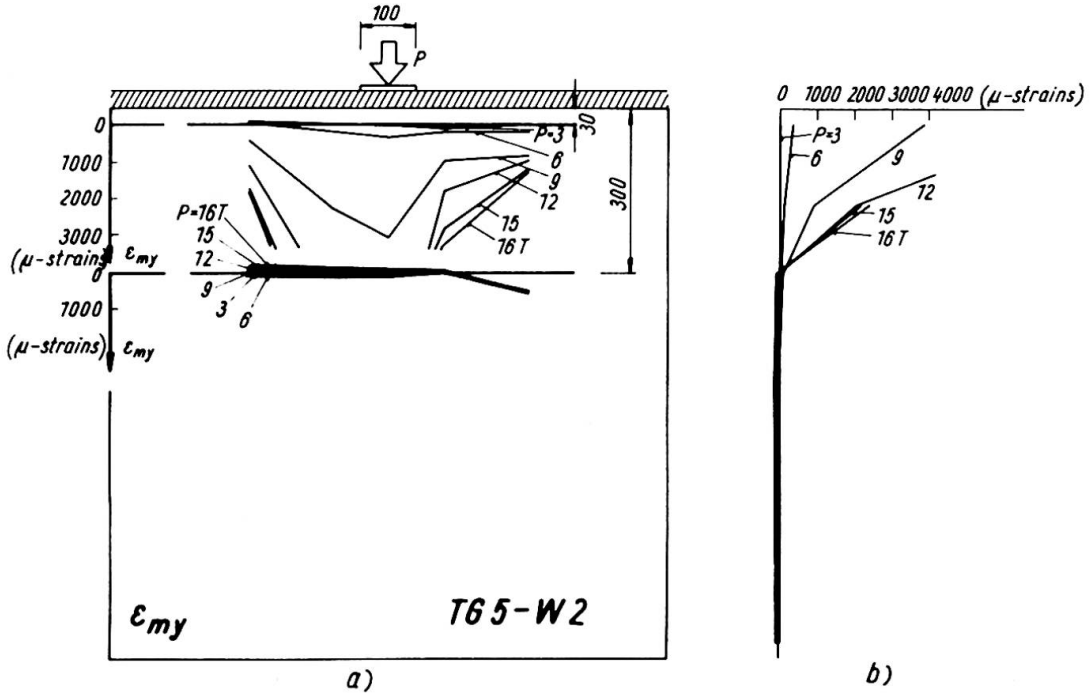

Fig. 6

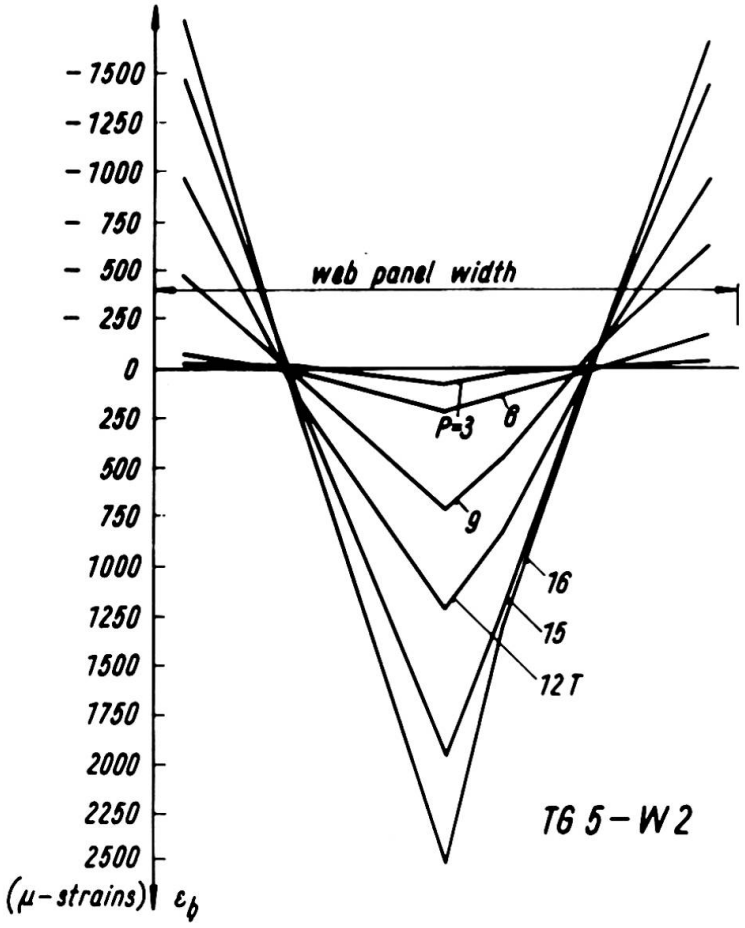

Fig. 7

flange of the same girder are plotted in Fig. 5.

The membrane strain distribution in web W 2 of girder TG 5 (heavy flanges) is shown in Fig. 6, the bending strains in the flange of the same girder are given in Fig. 7.

A comparison of the membrane strain patterns plotted in Figs. 4 and 6 again shows the considerable influence of flange inertia upon the post-buckled performance of the web. In the case of a girder with flexible flanges, the membrane stress pattern, like the buckled surface of the web discussed above, is localized in the neighbourhood of the partial edge load. Moreover, in this case are the strains still small for a load amounting to 90 % of the experimental load-carrying capacity. This indicates that the upper flange and the adjacent part of the web buckled inwardly (and the girder failed) before, or shortly after, the onset of yielding in the web. On the other hand, for a girder with rigid flanges, the stress pattern is wider (more distributed over the width of the web panel); and, even after the web has plastified in a considerable portion, the girder can sustain further load – thanks to the rigidity of the boundary framework consisting of the flanges and vertical stiffeners. Besides that, in this case the collapse of the girder is a slower process (and, therefore, not so dangerous a type of failure) than that which occurs with a girder having flexible flanges.

The ultimate loads P_{ult} of the test girders are given in Tables 1a, b, and the ratios P_{ult}/P_{cr}^{RB} (P_{cr}^{RB} denoting the critical load evoluated by Rockey's theory /5/, which takes account of flange dimensions) are plotted, in terms of the flange stiffness parameter I_f/a^3t and of the depth-to-thickness ratio $\lambda = b/t$ of the web, in Fig. 8. An analysis of the tables and figure indicates that thin webs subjected to a concentrated load, applied on to the upper flange between the vertical stiffeners of the web, manifest (like thin webs subjected to shear, bending and the like) a considerable post-critical reserve of strength, which ought to be taken into account in an optimum design of steel plate girders. This post-buckled strength grows with the depth-to-thickness ratio of the web and with the moment of inertia of the flange.

The effect of flange stiffness is very significant. For example, for girder TG 1, which had flexible flanges with

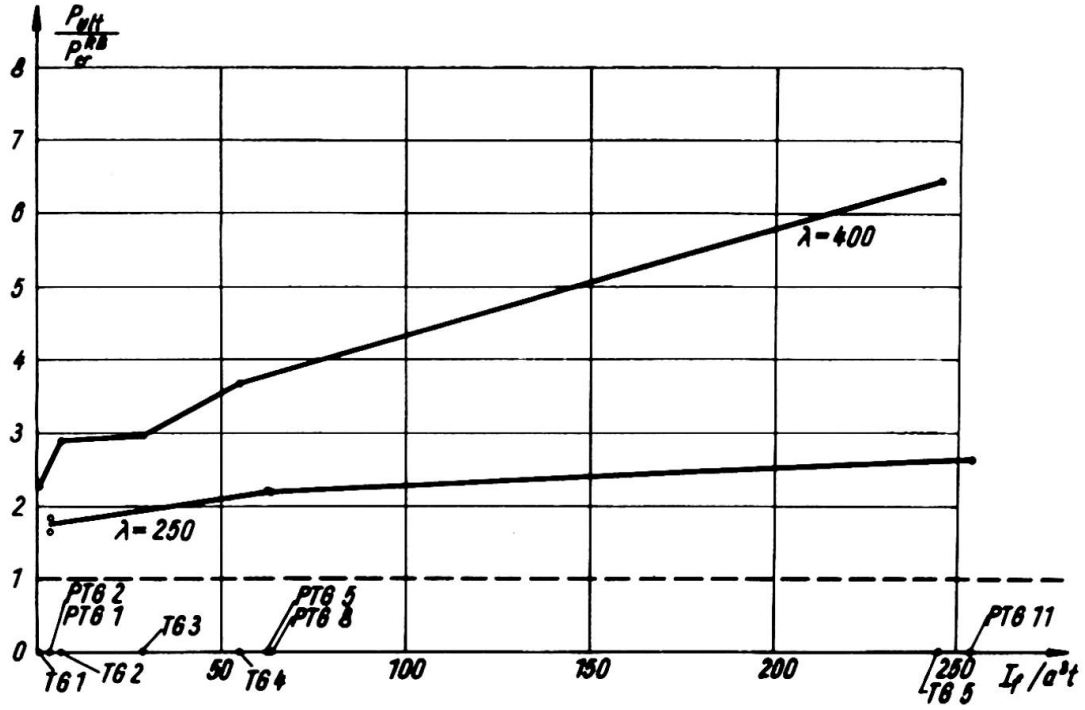

Fig. 8

I_f/a^3t = 0,89, the load-carrying capacity was 5 tons. On the other hand, for girder TG 5, having rigid flanges with I_f/a^3t = 254.4, the ultimate load attained 18 tons; which is 260% higher than the abovementioned collapse load of TG 1.

5. Cyclic Load Tests

The other part of the investigation dealt with "breathing" of the web, with stability of plastic post-critical web deflection and with incremental collapse.

The position of the concentrated load was the same as in the case of static tests; but the load cycled between 0.5 T and P_i , P_i denoting various loading steps. For each loading step, 1000 loading cycles were applied.

Three questions then needed replying:

(i) When a girder, subjected to a load cycling between 0.5T and an amplitude value P, operates in the plastic range, does an increase in web deflection occur during a certain number of loading cycles?

(ii) If it is so, do these deflection increments cease after a limited number of cycles of load applications?

(iii) Does the aforesaid deflection increase lead to a premature failure of the girder and to a reduction in its ultimate load, if compared to the value resulting from a static test?

Thanks to deflections and strains being measured carefully on an automatic recorder Ultralette, it was possible to give answers to the abovementioned questions.

An increase in web deflection (and strain) under a cyclic load was observed frequently in the plastic stage of the tests (see, for example, Fig. 9). This phenomenon "shook down", however, after a few (usually 3-5) cycles, the deflection

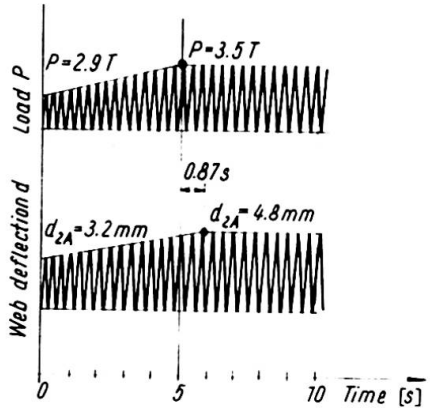

Fig. 9

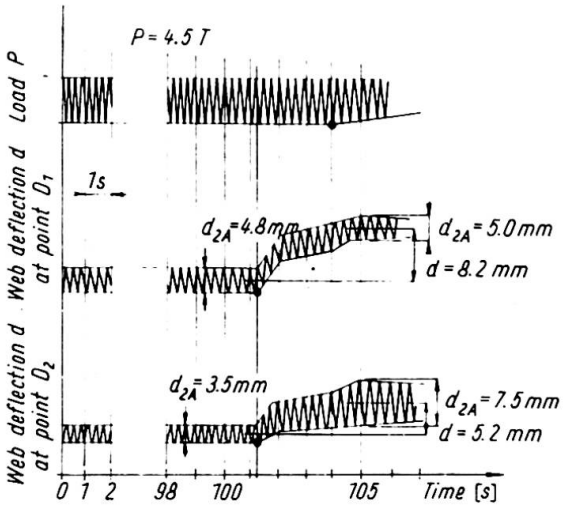

Fig. 10

stabilized, and the girder was able to sustain a higher load (Fig. 9). This happened for several successive loading steps; and only then the girder failed by deflection instability and incremental collapse (Fig. 10).

The failure loads P_{ult} resulting from the cyclic load tests are listed in Tables 1a, b and plotted, in terms of the flange stiffness I_f/a^3t and the depth-to-thickness ratio λ, in Fig.11.

In almost all tests, the cyclic ultimate loads were not lower than the load-carrying capacities resulting from the corresponding static experiments; and, in several cases, they were even higher. The cyclic loading and the incremental collapse did not, therefore, lead to any reduction in ultimate strength.

An inspection of Tables 1a, b and Fig. 11 also shows that the load-carrying capacities P_{ult} grew substantially with the flange stiffness, thereby demonstrating again the beneficial effect of flanges of great inertia.

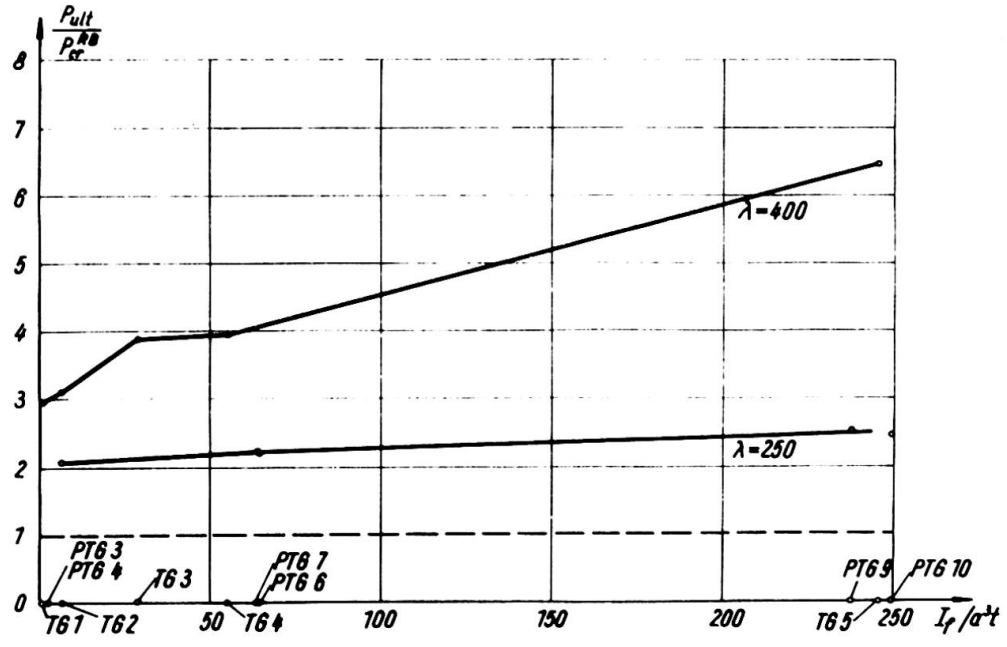

Fig. 11

Bibliography

/1/ Rockey, K.C., Škaloud, M.: The ultimate load behaviour of plate girders loaded in shear. Contribution presented at the IABSE Colloquium "Design of Plate and Box Girders for Ultimate Strength", London, March, 1971.

/2/ Škaloud, M.: Ultimate load and failure mechanism of thin webs in shear. dtto.

/3/ Bergreit, A.: Studies and tests on slender plate girders without stiffeners. dtto.

/4/ Bossert, T.W., Ostapenko,A.:Fritz Eng. Lab. Report No. 319.1, June, 1967.

/5/ Rockey, K.C., El-gaaly, M., Bagchi, D.: Buckling and ultimate strength of thin walled members when subjected to patch loading. University College Cardiff, 1971.

/6/ Novák, P., Škaloud M.: Experimental investigation into the post-buckled behaviour and incremental collapse of thin webs. Congress of RILEM, Buenos Aires, 1971.

/7/ Novák, P.: Méthode photostéréométrique dynamique des modèles. Colloque International de RILEM, Bucuresti, Septembre, 1969.

Summary

The paper deals with the ultimate load behaviour of thin webs subjected to a) static b) cyclic narrow partial edge load. An analysis of the experimental results shows that such webs (like those in shear, bending, etc.) posses a considerable post-buckled reserve of strength. It was also demonstrated that the post-critical behaviour and the ultimate load of the girder were very significantly affected by the flexural rigidity of flanges.